Mussel-Inspired Injectable Hydrogel Adhesive Formed under Mild Conditions Features Near-Native Tissue Properties

Kongchang Wei,[1,#] Berna Senturk,[2,#] Martin T. Matter,[3,4,5] Xi Wu,[6] Inge K. Herrmann,[3,4] Markus Rottmar,[2,] Claudio Toncelli[1,*]*

[1]Laboratory for Biomimetic Membranes and Textiles, [2]Laboratory for Biointerfaces,[3] Laboratory for Particles-Biology Interactions, Empa, Swiss Federal Laboratories for Materials Science and Technology, Lerchenfeldstrasse 5, 9014 St. Gallen, Switzerland; [4]Nanoparticle Systems Engineering Laboratory, Department of Mechanical and Process Engineering, [5]Particle Technology Laboratory, Institute of Process Engineering, Department of Mechanical and Process Engineering, ETH Zurich, Sonneggstrasse 3, 8092 Zurich, Switzerland; [6]Institute for Mechanical Systems, ETH Zürich, Leonhardstrasse 21, 8092 Zürich Switzerland.

Keywords: injectable hydrogel; tissue adhesive; tissue regeneration; mussel adhesion; biomimetic; enzymatic reaction

ABSTRACT

Injectable hydrogel adhesives, especially those that can strongly adhere to tissues and feature near-native tissue mechanical properties, are desirable biomaterials for tissue repair. Compared to non-adhesive injectable hydrogels for minimally invasive delivery of therapeutic agents, they can better retain the delivered agents at targeted tissue locations and provide additional local physical barriers. However, regardless of recent advances, an ideal injectable hydrogel adhesive with both proper adhesion and mechanical matching between hydrogels and tissues is yet to be demonstrated with cytocompatible and efficient *in situ* curing methods. Inspired by marine mussels, where different mussel foot proteins (Mfps) function cooperatively to achieve excellent wet adhesion, we herein report a dual-mode mimicking strategy by modifying gelatin (Gel) biopolymers with a single type thiourea-catechol (TU-Cat) functionality to mimic two types of Mfps and their mode of action. This strategy features a minor, yet impactful modification of biopolymers, which gives access to collective properties of an ideal injectable hydrogel adhesive. Specifically, with TU-Cat functionalization of only ~0.4 - 1.2 mol% of total amino acid residues, the Mfp-mimetic gelatin biopolymer (Gel-TU-Cat) can be injected and cured rapidly under mild and cytocompatible conditions, giving rise to tissue adhesive hydrogels with excellent matrix ductility, proper wet adhesion and native tissue-like stress relaxation behaviors. Such a set of properties originating from our novel dual-mode mimicking strategy makes the injectable hydrogel adhesive a promising platform for cell delivery and tissue repair.

1. Introduction

Hydrogels composed of three-dimensional polymer networks and a large amount of water are promising biomaterials due to their biochemical, structural and mechanical properties mimicking those of native tissues.[1-3] Among many hydrogels that have been developed since the 1960s,[4] injectable ones formed by *in situ* gelation feature additional advantages, including minimally invasive application and usability for irregularly shaped sites compared to their conventional pre-made counterparts.[5-8] Particularly, their capability in minimally invasive delivery of therapeutic agents, such as bioactive proteins and living cells, to desired tissue locations has attracted considerable interest.[9-14] Successful delivery and proper long-term functioning of such therapeutic agents require an ideal injectable hydrogel with a collective of unique properties.[15, 16] For instance, an optimum gelation rate is necessary for avoiding pre-gelation early loss of the therapeutic agents, proper tissue adhesion can prevent post-gelation displacement of the hydrogels, and good matrix ductility can minimize the brittleness and disintegration of the *in situ* formed hydrogels.[17] In addition, for cell delivery purposes, cytocompatibility of the precursor formulations, the crosslinking chemistry and also the injection method is indispensable, and the resulting hydrogels should ultimately provide a cell-instructive microenvironment that supports proper cellular functions such as cell attachment, spreading and migration.[12] Last but not least, the *in situ* formed hydrogels should also match the mechanical properties of native tissues in order to promote tissue regeneration.[18] However, despite the long-standing use of commercial tissue adhesives and recent advances of injectable biomaterials, it is still challenging to unify the aforementioned requirements for an ideal injectable hydrogel.[12, 19]

Commercial cyanoacrylate (CA, SuperGlue), which has been used a lot as a non-hydrogel form tissue adhesive, adheres strongly to tissue surfaces after injection, but is too cytotoxic for cell delivery and too rigid to accommodate soft tissue movement.[19] Fibrin glues (e.g. TISSEEL

from Baxter AG), as protein hydrogels, are more cytocompatible, but usually provide significantly weaker tissue adhesion than CA.[20] Polyethylene glycol (PEG)-based hydrogel adhesives (e.g. COSEAL from Baxter, DURASEAL from Confluent Surgical) are cytocompatible and provide tissue adhesion superior to fibrin glues.[21] However, the lack of cell interactions with PEG polymers hinders their application in cell-delivery for tissue regeneration.[8, 22] Recent advances in strong hydrogel adhesives have included tough alginate-polyacrylamide (Alg-PAAm) hydrogels,[19] highly adhesive gelatin methacryloyl (GelMA) hydrogels,[23] elastic human protein-based hydrogels,[24] and gelatin methacryloyl/hyaluronan (GelMA/HA-NB) hydrogels.[25] It is noteworthy that UV-initiated photopolymerization is commonly used for post-injection curing of these strong hydrogel adhesives. Inspired by marine mussels where different mussel foot proteins (Mfps) function cooperatively to achieve excellent wet adhesion, we herein report a dual-mode mimicking strategy with thiourea-catechol (TU-Cat) as the single type polymer functionality for mimicking two types of Mfps and their mode of action. Such a dual-mode mimicking strategy distinguishes the Gel-TU-Cat hydrogel adhesive in the current study from other mussel-inspired hydrogels that solely mimic the catechol-rich Mfps.

In nature, mussels produce catechol-rich adhesive mussel foot proteins (Mfps).[26] They stockpile them, and then eventually secrete and crosslink them to form byssal plaques that enable strong underwater adhesion.[27] In order to mimic the catechol-rich Mfps (e.g. Mfp-3 and Mfp-5 with catechol contents up to 15 mol% and 28 mol% of total amino acid residues, respectively), mussel-inspired polymers are typically functionalized with catechol moieties via non-reactive amides or ester linkages.[27, 28] Hydrogel formation can be induced by *in situ* oxidation of these catechol-functionalized polymers; therefore, no extra steps after injection (e.g. UV irradiation) are needed.[8, 28-31] However, with non-reactive linkages, the catechol-functionalized polymers usually need a long enzymatic crosslinking period (minutes) to form hydrogels under basic conditions.[29] Although using strong oxidants such as sodium periodate

($NaIO_4$) could shorten it to less than 1 minute, the harsh oxidizing condition could limit its application in cell delivery.[30, 32, 33] Recent investigations on mussel adhesion have revealed that, besides catechol-rich Mfps, thiol-rich Mfp-6 also plays an important role in the rapid gelation and remarkable adhesion of mussels (Figure 1A).[34-38] Although Mfp-6 contains only ~3 mol% of catechols, its cysteine residues not only rapidly crosslink the catechol-rich proteins (e.g. Mfp-3 and Mfp-5), but also reduce the oxidized transient products (quinones) back to catechols.[34] It is with such a cooperative pathway that the Mfps establish the strong mussel adhesion (Figure 1C). Notably, by mimicking a combination of catechol-rich Mfps and thiol-rich Mfp-6, new mussel-inspired hydrogels with faster gelation behavior or better adhesion performance have been recently developed.[38, 39] Like in mussels, crosslinking of catechol-functionalized polymers by nucleophilic thiourea (TU) functionalities resulted in rapid formation of hydrogels and preservation of the adhesive catechol structures under a broad range of pH (pH 2-10), which was not found from TU-free catechol-functionalized polymers.[39] These hydrogels can adhere strongly to inorganic substrates. However, strong oxidants ($NaIO_4$) used in the study limits the applicability of the system to *ex vivo* applications.[39] Extension to applications related to living cells or biological tissues has yet to be demonstrated following the establishment of milder crosslinking conditions. In the current study, we demonstrate that gelation polymers modified with a small amount of the dual-mode mimicking thiourea-catechol (TU-Cat) functionality can be enzymatically cross-linked rapidly under exceptionally mild and cell-friendly conditions. The resulting mussel-inspired hydrogels (Gel-TU-Cat hydrogels) feature tissue adhesive and near-native soft tissue properties. Specifically, the development and characterization as well as the *in vitro* and *ex vivo* evaluation of such an injectable Gelatin-TU-Cat hydrogel tissue adhesive are presented.

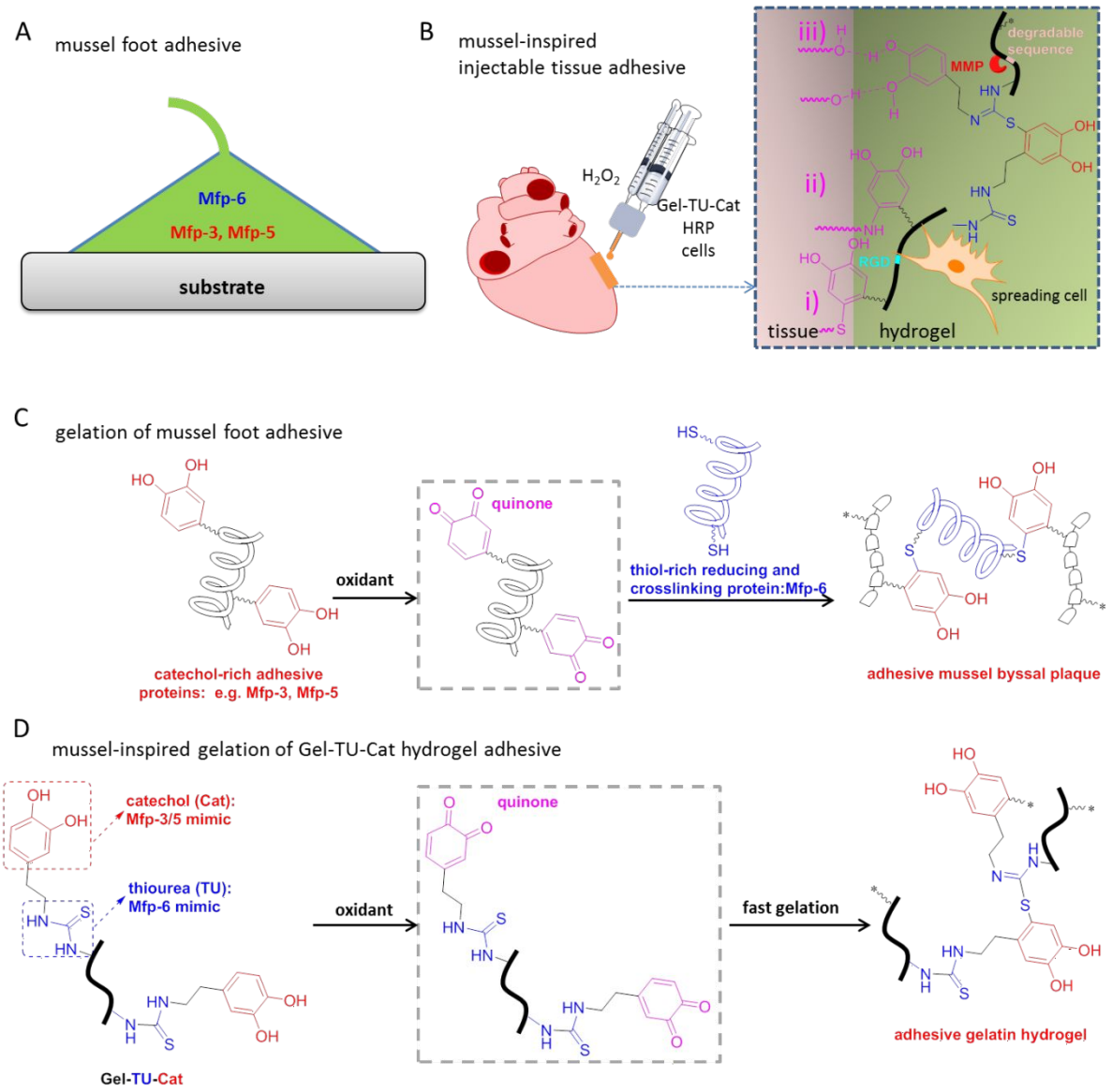

Figure 1. Schematic illustration of the mussel-inspired injectable Gel-TU-Cat hydrogel tissue adhesive. (A) Schematic of mussel foot proteins (Mfps) involved in strong mussel-substrate adhesion. (B) Relevant interfacial interactions (highlighted by pink structures: i. thiol-catechol addition, ii. amine-catechol addition and iii. hydrogen bonding) and cell spreading due to the presence of RGD and MMP-degradable sequence. (C) The formation of the adhesive mussel byssal plaques from catechol-rich adhesive proteins (e.g. Mfp-3 and Mfp-5) and thiol-rich reducing and crosslinking protein Mfp-6. (D) The biomimetic formation of crosslinked and adhesive Gel-TU-Cat hydrogel adhesive, of which the catechol (Cat) moieties mimic the adhesive function of Mfp-3 and Mfp-5, and the thiourea (TU) linkages mimic the reducing and crosslinking function of Mfp-6.

2. Experimental section

2.1 Materials. Gelatin from porcine skin (gel strength 300, type A), dopamine hydrochloride (DOPA, as a white powder), sodium sulfate anhydrous (Na_2SO_4), triethylamine (TEA, ≥ 99.5%), carbon disulfide (CS2, ≥ 99.9%), hydrogen peroxide solution (H_2O_2, containing inhibitor, 30 wt% in H_2O, ACS reagent), peroxidase from horseradish (HRP, Type VI, essentially salt-free, lyophilized powder, ≥ 250 units/mg solid), deuterated dimethyl sulfoxide (DMSO-*d6* with 99.96 atom %D), hydrochloric acid (HCl, ACS reagent, 37 wt%) and dimethyl sulfoxide (DMSO, ≥ 99%) were purchased from Sigma-Aldrich. Tetrahydrofuran (THF, ≥ 99%) and methanol (≥ 99%) were purchased from Fisher Chemical. All chemicals were used as received unless specified otherwise.

High glucose Dulbecco's Modified Eagle Medium (DMEM), fetal bovine serum (FBS), penicillin-streptomycin-neomycin (PSN), L-glutamine, paraformaldehyde (4%), phosphate-buffered saline (PBS), Triton X-100, bovine serum albumin (BSA), calcein-AM, propidium iodide (PI) were purchased from ThermoFisher Scientific. Phalloidin 633 (Alexa Fluor® 633 phalloidin) was purchased from Molecular Probes. The Pierce Lactate dehydrogenase (LDH) Cytotoxicity Assay Kit and 4′,6-diamidino-2-phenylindole (DAPI) were purchased from Sigma-Aldrich.

The double syringe biomaterial delivery K-system with a total volume of 2.5 mL and the volume ratio of 4:1 between syringes was purchased from Medmix (Medmix Systems AG, Switzerland). Dry regenerated cellulose (RC) membranes (Spectra/Por® 1, 6-8 kD MWCO) were purchased from Faust (Switzerland). Polytetrafluoroethylene (PTFE) films with thickness of 1 mm for the fabrication of molds were purchased from Sigma-Aldrich. Polyethylene terephthalate (PET) films for backing of the T-peeling testing specimens were purchased from 3M Italia S.p.A. Fresh porcine hearts were obtained from the local slaughterhouse (Slaughterhouse St. Gallen AG, operation Bazenheid).

2.2 Synthesis of thiourea-catechol functionalized gelatin (Gel-TU-Cat). 4-(2′-isothiocyanatoethyl)-1,2-benzenediol (DOPA-ITC) was firstly synthesized according to a previously reported procedure with slight modifications.[40] DOPA (5.0 g, 26.4 mmol) was partially dissolved in tetrahydrofuran (80 mL) with stirring before TEA (4.4 mL, 31.6 mmol) was added. Methanol (80 mL) was added to dissolve DOPA. CS_2 (8.0 mL, 131.9 mmol) was added to the mixture and stirred for 30 minutes at 25 °C under nitrogen atmosphere. The reaction mixture was cooled with an ice bath before H_2O_2 (6.2 mL, 74.9 mmol) was added dropwise. The solution was immediately acidified with HCl (2.64 mL) and then concentrated with a rotary evaporator (at 23 °C, under 300 mbar and 100 rpm). The resulting mixture was filtered and washed with deionized water (DI water). The filtrate was extracted with ethyl acetate three times (3 × 50 mL). The combined organic layers were dried by Na_2SO_4 overnight under argon protection. After filtration, the solution was concentrated with a rotary evaporator (at 40 °C, under 200 mbar and 100 rpm) to give the product as oil. The crude product was characterized by ^{1}H NMR (Figure S1) before its use for functionalization of gelatin. Gelatin (5.0 g) was dissolved in a mixture of DI water/DMSO (1:1, 200 mL) at 37 °C. Then selected amounts of DOPA-ITC (0.5g, 1.5g, or 2.5 g) were added to the mixture under nitrogen atmosphere to achieve different functionalization degrees. The solution was left stirring for 12 hours at 37 °C under nitrogen protection. The resulting solution was purified by dialysis (MWCO 6-8 kDa) against DMSO for two days and then against DI water for four days at 37 °C before lyophilization to give the products Gel-TU-Cat-L, Gel-TU-Cat-M and Gel-TU-Cat-H polymers, where L, M and H indicates the low, medium and high functionalization degree of the Gel-TU-Cat polymers, respectively.

2.3 Quantification of the catechol contents by UV-vis absorbance. A Cary 50 Bio UV-vis spectrophotometer was used for all UV-vis absorbance measurements. A standard curve was made with gelatin solutions (1 mg/mL) in the presence of different amounts of DOPA-ITC (0.02, 0.04, 0.06, 0.08 and 0.10 mg/mL). The UV-vis absorbance of Gel-TU-Cat solutions (1

mg/mL) at the wavelength of 282 nm was used to calculate the catechol content of the Gel-TU-Cat polymers from the standard curve (Figure S2, Table S1 and Table S2).

2.4 Conversion rate of ε-amino groups or total amino acid residues to TU-Cat functionalities. The conversion rates were calculated with the Equation 1 and Equation 2, where $R_{\varepsilon\text{-}amino}$ is the conversion rate of ε-amino groups and R_{total} is the conversion rate of total amino acid residues. C_{Cat} is the catechol content of the synthesized Gel-TU-Cat polymers determined by the method described in section 2.3. Cε-amino is the ε-amino content of Type A porcine gelatin as reported elsewhere (286 μmol/g gelatin),[41] which corresponds to 28.6 ε-amino groups per 1000 amino acid residues.

$$R_{\varepsilon\text{-amino}} = C_{Cat}/C_{\varepsilon\text{-amino}} \quad \text{(Equation 1)}$$

$$R_{total} = R_{\varepsilon\text{-amino}} \times 28.6/1000 \quad \text{(Equation 2)}$$

2.5 Preparation of Gel-TU-Cat hydrogels. H_2O_2 concentration has been considered as the critical cytotoxic parameter of HRP/H_2O_2 crosslinking systems.[44] In order to minimize the cytotoxicity of the hydrogel formulation, the enzymatic crosslinking condition was optimized for fast gelation at minimal H_2O_2 concentration. To determine the lowest concentration for fast gelation, we have tested different final concentrations of H_2O_2, ranging from 0.1 – 5.0 mM, with a fixed HRP concentration of 5 units/mL. As shown in Figure S3, gelation within the first two minutes was insufficient for H_2O_2 concentrations ≤ 3 mM. H_2O_2 concentrations of 5mM and 5 units/mL HRP were eventually used for the further experiments as these unify favorable gelation properties with cytocompatibility (see also Section 2.11-12). Typically, a mixed solution (0.8 mL) containing Gelatin-TU-Cat (100 mg) and HRP (20 μg) was prepared in PBS at 37 °C, and H_2O_2 was diluted by PBS to the concentration of 25 mM at room temperature. The mixed solutions of Gel-TU-Cat/HRP and the PBS solution of H_2O_2 were loaded into the double syringe biomaterial delivery K-system. The mixed solution of Gel-TU-Cat/HRP was loaded in the 2 mL syringe and the PBS solution of H_2O_2 was loaded in the 0.5 mL syringe of

the K-system. By injecting both solutions through the mixing tip of the K-system, hydrogels were formed on targeted locations. After injection, the final concentration of Gelatin-TU-Catwas 100 mg/mL.

2.6 Scanning electron microscopy (SEM). Scanning electron microscopy images were taken with a Hitachi S-4800 model (Hitachi-High Technologies, Illinois), with acceleration voltage of 2 kV and a current flow of 10 μA. Hydrogel thin films were prepared as described in section 2.5 with PTFE molds (diameter 15 mm, thickness 1 mm), and then frozen with liquid nitrogen. After lyophilization, the samples were sputter-coated with a layer of gold-palladium (7 nm thick, EM ACE600, Leica Microsystems, Switzerland) before being imaged with SEM.

2.7 Rheological measurements. A MCR301 rheometer (Anton Paar) equipped with a plate-plate Toolmaster system (PP25-SN21182) was used for all measurements. Gelatin solutions or Gel-TU-Cat hydrogels were prepared and deposited on the testing plate as described in section 2.5 and loaded on the rheometer. The oscillatory time-sweep measurements (strain 1%, frequency 1 Hz) were initiated at 90 seconds after samples were deposited on the testing plate. For oscillatory rheological frequency-sweep measurements, the strain was kept at 1%. For shear stress-relaxation experiments, the strain was varied from 10% to 90%.

2.8 Unconfined compressive tests. Unconfined compressive tests were carried out on a MCR301 rheometer (Anton Paar) equipped with a plate-plate system (PP25-SN21182). The testing program was adapted from a common oscillatory time test program (Time Test Oscillation /CSD), where strain and frequency were fixed at 0.001% and 0.001 Hz, respectively. The loading speed was kept at 3mm/min. For cyclic compressive tests, the same program was used with an additional unloading step (the unloading speed was set -3mm/min).

2.9 Quantification of the adhesion energy by T-peeling tests. This study was carried out by following the ASTM F2256-05 standard protocol with minor changes made specifically for hydrogel systems.[19] Firstly, rectangle pericardium tissues with dimensions around 70 × 20 × 4 mm (length × width × thickness) were carefully peeled off from fresh porcine hearts at room

temperature (Figure S4A). They were then glued to PET films with similar dimensions (Figure S4B). Two pieces of the PET-backed tissues were adhered to each other after direct injection of the CA, TISSEEL or Gel-TU-Cat hydrogel adhesives on the tissue surface. A PTFE film (20 × 10 × 1 mm in terms of length × width × thickness) was placed at one end of the specimen between two tissue surfaces in order to create the open end of the specimen. The specimens were further cut to adjust the shapes, so that the two pieces of tissues in one specimen have the same dimensions (Figure S4C). To avoid dehydration of the tissues during the specimen preparation, the tissues were kept in PBS at room temperature before use. The prepared specimen was then fixed on custom-built setup (MTS Systems, Eden Prairie, MN, USA) consisting of horizontal hydraulic actuators equipped with force sensors with a capacity of 50 N (Figure S4D). The displacement and pulling force was recorded during peeling with a speed of 100 mm/min at room temperature. The adhesion energy was calculated as two times the averaged plateau value of the ratio of the force and width (F/W).[19]

2.10 Bursting strength measurements. The bursting strength measurements were carried out by following the ASTM F2392 standard protocol with minor changes made specifically for hydrogel systems.[19] Firstly, the pericardium tissues with a thickness between 3 to 5 mm were carefully peeled off from fresh porcine hearts (Figure S5A). A penetrating defect (3 mm in diameter) was then created with a biopsy puncher at the center of the tissue. This tissue substrate was placed in between two PTFE plates (thickness: 1 mm), of which the upper one displaying a hole of 15 mm in diameter was used as the mold for hydrogel formation (Figure S5B). Two minutes after the hydrogel (as described in section 2.5) was deposited, the tissue substrate with the hydrogel-sealed defect was fixed in the testing chamber prefilled with PBS (Figure S5C-D). The pressure was increased by pumping PBS at a speed of 2 mL/min with a Cetoni Low Pressure Syringe Pump neMESYS 290N. During the measurement, the pressure was recorded and the bursting pressure was determined as the pressure that was required to burst the hydrogels.

2.11 Normal human dermal fibroblast (NHDF) cell encapsulation in Gel-TU-Cat hydrogels. NHDFs purchased from CELLnTEC (juvenile donor) were expanded in DMEM supplemented with 10% FBS, 1% PSN, 1 % L-glutamine and used at passages 4-5. Cell-laden hydrogels were prepared with a similar procedure as described in section 2.5. Before being loaded into the double syringe biomaterial delivery K-system, NHDFs were thoroughly suspended in the mixed solution of Gel-TU-Cat-M/HRP. The disk-like cell-laden hydrogels (1 mm in thickness and 6 mm in diameter) were formed by injection into a customized PDMS mold as shown in Figure S6 and transported to the cell culture plates after 2 minutes. The cell density was kept as 2×10^5 cells/mL for each hydrogel disk (~5700 cells/gel). The glass slides supporting the PDMS mold during hydrogel preparation (Figure S6) were pre-treated with Sigmacote to minimize hydrogel-glass adhesion.

2.12 3D cultivation and confocal microscopic observation of NHDFs in Gel-TU-Cat hydrogels. The cell-laden hydrogels were cultivated in high glucose DMEM medium supplemented with 10% FBS, 1% PSN and 1 % L-glutamine. The medium was refreshed every two days. To assess cell attachment and spreading, at selected days, the cells were fixed in 4% paraformaldehyde for 30 min, washed with PBS and permeabilized in 0.1% Triton X-100 for 30 min at room temperature. Subsequently, samples were washed 2 times with PBS and then immersed in 1% BSA solution for 30 min to block unspecific binding. The hydrogel samples were rinsed again with PBS and stained with phalloidin 633 (Alexa Fluor® 633 phalloidin, 1:200 dilution) and DAPI (1:4000 dilution) in 1% BSA on a shaker for 2 h in the dark. The samples were rinsed twice with 1% BSA and twice with PBS before imaging. For the live/dead assay, cell-laden hydrogels were washed with PBS and then incubated in PBS containing 0.1 vol% calcein-AM and 0.1 vol% propidium iodide (PI) for 20 min. As dead cell control of the live/dead staining assay (Figure S7), cell-laden hydrogels were incubated in the culturing medium containing 0.2 wt% digitonin detergent for 5min at 37 ºC prior to staining procedure

(a stock solution of 2 wt% digitonin in PBS was prepared beforehand by heating at 95 ºC for 5 min). The samples were imaged by a laser confocal microscopy (LSM780, Carl Zeiss).

2.13 LDH release assay. While various assays can be used for cytotoxicity studies, cell proliferation assays (such as MTT, MTS, etc) typically measure the metabolic activity, but cannot distinguish the effects of cell death or cell growth inhibition. Lactate dehydrogenase (LDH) assay provides a simple and reliable method for determining the extent of cell death or growth inhibition caused by cytotoxicity.[42,43] To assess and quantify potential cytotoxic effects of the hydrogels, the release of LDH from NHDFs was measured using a CytoTox 96 assay (Promega) according to the manufacturer's instructions. In brief, the cell-laden hydrogel disks were prepared as described in section 2.11 and cultivated as described in section 2.12. Before collecting the supernatant of the hydrogel scaffolds at day 1, 3 and 7, 50 µL of lysis solution were added to one control group containing 500 µL medium and incubated for 45 min to prepare a maximum LDH release condition as positive control. After collecting the supernatants, 50 µL CytoTox 96 Reagent were added to the collected supernatant (50 µL) and shaken in the dark for 30 min. After adding 50 µL of Stop Solution to all samples, absorbance was measured at 490 nm using a Mithras LB 943 Multimode Microplate Reader (Berthold Technologies, Germany).

2.14 Statistical analysis. Data were presented as mean ± standard deviation (SD). For the characterization of mechanical properties, including elastic modulus, adhesion energy and bursting pressure, one-way ANOVA was used for comparing differences between groups, followed by a post hoc t-test (Two-Sample Assuming Equal Variance). For LDH release assay, two-way ANOVA was used for comparing differences between groups, followed by Tukey's post hoc test.

3. Results and Discussion

3.1 Synthesis, characterization and enzymatic crosslinking of Gel-TU-Cat polymers

Thiourea-catechol (TU-Cat) functionalized gelatin polymers with three different functionalization degrees were synthesized according to a previously reported approach (Figure 2A and Figure S1).[39] The detailed formulations are listed in Table 1. With increasing feeding ratio between DOPA-ITC and gelatin, the functionalization degree of modified gelatin polymers increased as evidenced by ^{1}H NMR (Figure 2B). The integration of aromatic signals within the 6.9-7.3 ppm (*y* region) was calibrated to the integration of pristine gelatin aromatic signals located at 7.6-7.8 ppm (*x* region). According to the increasing integration of the *y* region, the three polymers with low, medium and high functionalization degree were termed as Gel-TU-Cat-L, Gel-TU-Cat-M and Gel-TU-Cat-H, respectively (Figure 2B and Table 1). Their catechol contents were quantified with a UV-vis standard curve as described in Section 2.4 (Figure S2, Table S1 and Table S2) and the results are summarized in Table 1. As shown in Table 1, only around 42.3 mol% of ε-amino groups, or 1.2 mol% of total amino acid residues, were converted to TU-Cat functionalities even when an excessive DOPA-ITC (7.5 *equiv.* to ε-amino groups) was introduced to produce Gel-TU-Cat-H polymers.

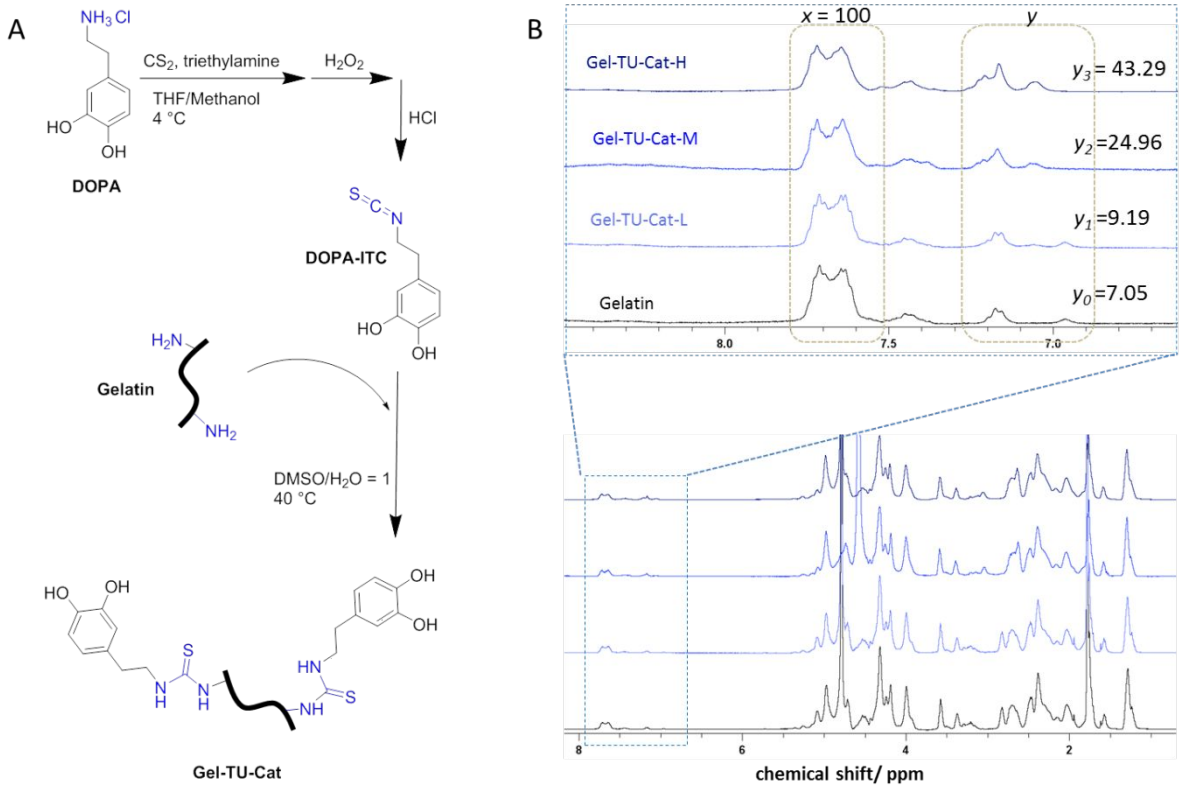

Figure 2. (A) Synthesis of Gel-TU-Cat polymers. (B) ^{1}H NMR characterization of gelatin and Gel-TU-Cat polymers (in D_2O, 37°C) with different functionalization degrees.

Table 1. Synthesis and characterization of Gel-TU-Cat polymers.

	Reactant concentrations[a]				^{1}H NMR Integration[b]			Catechol content[c]	Conversion	
	Gelatin	ε-amino	DOPA-ITC		*x*	*y*	Δ*y*	Mean ± SD	ε-amino[d]	Total[e]
Units	g	mmol	g	mmol	/	/	/	μmol/g	mol%	mol%
Gel-TU-Cat-H	5.0	1.7	2.5	12.8	100	43.29	514%	120.9± 0.2	42.3	1.2
Gel-TU-Cat-M	5.0	1.7	1.5	7.7	100	24.96	254%	55.2± 0.1	19.3	0.6
Gel-TU-Cat-L	5.0	1.7	0.5	2.6	100	9.19	30%	36.5± 0.5	12.8	0.4
Gelatin	/	/	/	/	100	7.05	0%	/	/	/

[a.] Different feed ratios between gelatin and DOPA-ITC were used for synthesizing Gel-TU-Cat polymers. [b.] The calculation was based on the ^{1}H NMR spectra in Figure 2B, where the integration of area *x* was fixed as 100, the increase of the integration of *y* was attributed to the conjugation of DOPA-ITC to gelatin, $\Delta y=(y-y_0)/y_0$. [c.] Catechol contents of the synthesized Gel-TU-Cat polymers were determined by UV-vis measurements with a standard curve as described in the supporting information Figure S2. [d.] The percentage of ε-amino groups converted to TU-Cat groups. [e.] The percentage of total amino acid residues converted to TU-Cat groups.

Although strong oxidants such as $NaIO_4$ can effectively induce the crosslinking of catechol-functionalized polymers, the cytotoxicity impairs the application in cell encapsulation and 3D cell culturing.[39, 44] Here, we introduce HRP and H_2O_2 for enzymatic crosslinking of the Gel-TU-Cat polymers, in analogy to the HRP/H_2O_2 systems used for the crosslinking of tyramine-functionalized polymer hydrogels.[45] HRP/H_2O_2 crosslinking conditions are well tolerated by cells, thus rendering the Gel-TU-Cat gel system suitable for cell encapsulation and 3D cell culturing for tissue engineering.[46] As suggested for biomedical application of HRP-catalyzed hydrogels,[46] the Gel-TU-Cat polymer solution was firstly mixed with HRP before gelation was triggered by H_2O_2. Although the overall change of the gelatin backbone is minor, especially for the Gel-TU-Cat-L polymers where only 0.4 mol% of the total amino acid residues were converted to TU-Cat groups, it significantly altered the gelation behavior of gelatin at 37 °C when HRP and H_2O_2 were used as enzymatic crosslinking agents. As revealed by the qualitative tube inversion test,[47] when the Gel-TU-Cat-L solution was mixed with HRP and H_2O_2 with the

double syringe biomaterials delivery K-system (Section 2.5), the hydrogel was formed within 10 seconds. On the contrary, no hydrogel was formed from gelatin under the same condition (Movie S1). The gelation process was also characterized by oscillatory rheology time sweep measurements (Figure 3A and Figure S8A). Although the gelation of Gel-TU-Cat-L and Gel-TU-Cat-M was still proceeding as indicated by the increasing modulus (elastic modulus G', loss modulus G''), the crosslinking reaction was completed within 10 min (Figure S8B). Such a mild but efficient crosslinking system enables direct injection molding of hydrogel objects, with the prospects of direct applicability to living tissues. As demonstrated in Figure 3B-D, sophisticated surface features can easily be transferred from a mold to the hydrogel object. This freeform moldability indicates that such injectable hydrogels can be useful to seal irregular tissue defects, potentially also *in situ*. In addition, the final mechanical properties of the Gel-TU-Cat hydrogels could be controlled by the catechol contents (Figure S8B), polymer (Figure S9A) and H_2O_2 concentration (Figure S9B) as confirmed by their plateau modulus. SEM analysis revealed the micro-structures of the lyophilized Gel-TU-Cat hydrogels. Although lyophilization can affect the micro-structures, the relative morphological difference indicates a fundamental micro-structural difference between samples prepared with the same drying process.[48] The SEM results reflect the difference between the hydrogels prepared from polymers with different functionalization degrees (Figure 3E). With higher functionalization degree, Gel-TU-Cat-M hydrogels show smaller pores than Gel-TU-Cat-L. Particularly, the most uniform distribution of micro-pores was found in Gel-TU-Cat-M hydrogels. The medium catechol functionalization degree of the Gel-TU-Cat-M polymers is likely to support suitable gelation kinetics, which leads to homogeneous crosslinking.[48-50] No interconnected pores but fringes on the surface were observed for Gel-TU-Cat-H hydrogels. This may reflect the least porous structures of Gel-TU-Cat-H hydrogels corresponding to the highest functionalization degree. By slowing down the gelation process at lower HRP and H_2O_2 concentrations, structure that is more porous was observed from Gel-TU-Cat-H hydrogels (Figure S10).

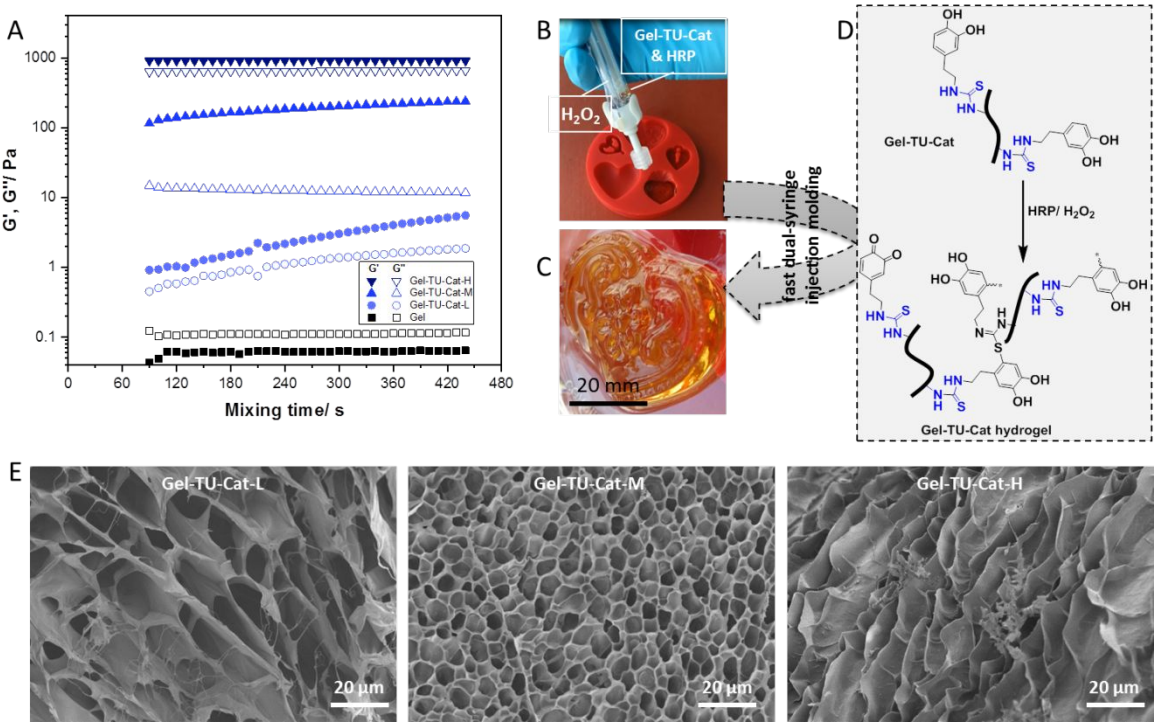

Figure 3. (A) Gelation of Gel-TU-Cat polymers characterized by rheological time sweep measurement. (B-D) Fast double-syringe injection molding of Gel-TU-Cat-M into a heart shaped object with sophisticated surface features from the mold. (E) SEM images showing the effect of functionalization degree on micro-structures of Gel-TU-Cat hydrogels.

3.2 Mechanical properties of Gel-TU-Cat hydrogels

Further examination of the mechanical properties of Gel-TU-Cat hydrogels by oscillatory frequency sweep confirmed the covalent crosslinking of the TU-Cat modified gelatin polymers (Figure 4A). At physiological temperature (37 °C), following enzymatic oxidation the Gel-TU-Cat hydrogels demonstrated higher G' than G", and negligible frequency dependency of both G' and G'' within the frequency range of 0.01-10 Hz, therefore behaving as hydrogel. In contrast, native gelatin showed a higher G" than G'. This characteristic higher G' compared to G" characteristic for stable chemical hydrogels indicates that TU-Cat functionalities along the Gel-TU-Cat polymer backbones are responsible for the covalent crosslinking of the polymers. Additionally, non-covalent interactions in catechol-containing systems, such as hydrogen bonding and π-π stacking,[36, 37] provide sacrificial crosslinks and thus improve the hydrogel

matrix ductility (Figure 4B). Unlike conventional chemical biopolymer hydrogels, which are usually brittle and withstand less than 10% of shear strain,[51, 52] Gel-TU-Cat hydrogels are considerably less brittle as evidenced by their broad linear viscoelastic (LVE) ranges (up to 100% shear strain). In addition to the improved ductility, the low damping factor (DF = G''/G' < 0.1) indicates good elasticity of the Gel-TU-Cat hydrogels. Similar behavior has also been reported in many covalent/non-covalent hybrid crosslinking hydrogels (Figure 4C).[53-55] It is noteworthy that the Gel-TU-Cat hydrogels use solely a single type of functionality (TU-Cat) and a single step for establishing both covalent and noncovalent interactions, which distinguishes them from other hybrid crosslinking hydrogels that usually involve multiple chemical functionalities and curing steps for establishing different types of crosslinking.[53-55] Such an elegant and effective strategy for combining good ductility and elasticity of hybrid crosslinking hydrogels opens up new opportunities for application in tissue repair, especially for tissues with continuous dynamic movements such as hearts and lungs.

To further demonstrate the hybrid crosslinking nature (Figure 4C), the shear stress relaxation of Gel-TU-Cat-M hydrogels under different strains (10-90%) was examined (Figure 4D). As described by the Maxwell-Weichert model with two spring-dashpot Maxwell elements in parallel, the stress relaxation of hybrid crosslinking hydrogels can be well fitted with double exponential decay (ExpDecay2 function from Origin), giving two characteristic relaxation times (τ_1 and τ_2) of the hydrogel ($R^2 = 0.989 \pm 0.006$, Supporting information: Supplementary Note 1 and Table S3).[56, 57] The fast stress relaxation mode originating from non-covalent crosslinking had a much shorter characteristic relaxation time τ_1 (6.46 ± 0.96 s) than the slow mode that originates from the covalent crosslinking (τ_2 = 364.47 ± 47.18 s). This double-exponential stress relaxation behavior has also been observed in muscle-mimicking hydrogel materials,[58, 59] highlighting the importance of such a feature in load-bearing biomaterials. Like muscles, such hydrogels can prevent early breakage by relaxing the initial stress rapidly with a fast mode originating from sacrificial crosslinks, thus withstanding large deformations.[55, 58-61]

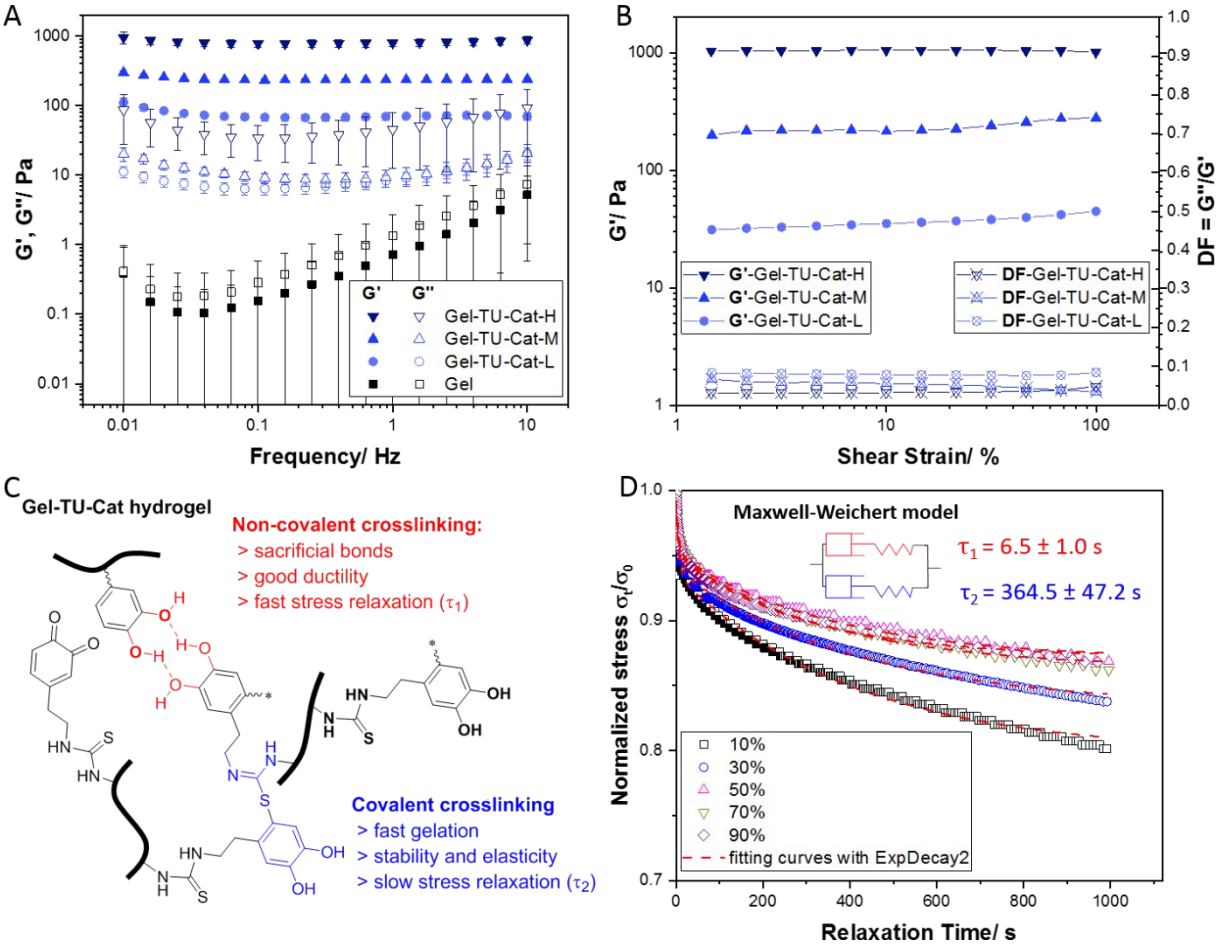

Figure 4. (A) Dynamic oscillatory rheological frequency-sweep measurements of Gel-TU-Cat or gelatin under enzymatic oxidation (n=3). (B) Dynamic oscillatory rheological amplitude-sweep measurements of Gel-TU-Cat hydrogels. (C) Schematic illustration of covalent and non-covalent hybrid crosslinking of the Gel-TU-Cat hydrogels. (D) Shear stress relaxation of Gel-TU-Cat-M hydrogels under different strains (10-90%) described by the Maxwell-Weichert model with two spring-dashpot Maxwell elements in parallel. The stress relaxation curves were fitted with double exponential decay, giving two characteristic relaxation times (τ_1 and τ_2) of the hydrogel. The rheological and stress relaxation measurements were carried out at 37 °C.

The hybrid crosslinking nature of Gel-TU-Cat hydrogels and their good matrix ductility were also evidenced by the large compressive deformations that they can withstand (Figure 5A). No breakage was observed from Gel-TU-Cat-L and Gel-TU-Cat-M hydrogels, only Gel-TU-Cat-H hydrogels were internally fractured before reaching the compressive strain of 80%.

Nevertheless, all the disk-like hydrogels retained their macroscopic integrity after being compressed to such a large strain (Figure 5A inset). Dissipation of the loading energy enabled by the sacrificial non-covalent interactions was revealed by the mechanical hysteresis of the hydrogels (Figure 5B), as was also reported for other hybrid crosslinking hydrogels.[53, 54, 62] Under consecutive cyclic compressions, nearly identical hysteresis loops were found for the first and second cycles of Gel-TU-Cat-L and Gel-TU-Cat-M hydrogels. This indicates that the chemical crosslinks are loosely distributed within these two hydrogel matrices, and they were barely affected during the cyclic compressions. This is reasonable since the overall catechol content of Gel-TU-Cat-L and Gel-TU-Cat-M polymers is low (Table 1). However, Gel-TU-Cat-H hydrogels with higher chemical crosslinking densities were not able to fully dissipate the loading energy by sacrificial non-covalent interactions. In addition to the temporal dissociation of non-covalent bonds, partial disruption of the chemical crosslinks occurred during the first cycle, thus compromising the mechanical strength in the second cycle (Figure 5B and Figure S11).

Furthermore, the mechanical strength of the Gel-TU-Cat hydrogels was also quantified under small deformations. The Young's modulus (E) was calculated from the linear fitting of the initial part of the compressive stress-strain curves with strains below 0.25 (Figure 5C, Supporting information Supplementary Note 2 and Table S4), and summarized along with the catechol contents ([Cat] μmol/g polymer) in Figure 5D. It can be clearly seen that the Young's modulus can be adjusted by the catechol contents of the polymers. More importantly, the soft nature of Gel-TU-Cat hydrogels ($E \approx 3$-18 kPa) matches well with soft tissues such as muscles ($E \approx 5$-15 kPa).[63] Such matching of mechanical properties between biomaterials for tissue repair and native soft tissues has already been found of crucial importance in many aspects.[18] Better matching of the mechanical properties not only promotes the directed differentiation of encapsulated stem cells into desired phenotypes,[64] but also minimizes the mechanical irritation towards the surrounding tissues, therefore better supporting tissue repair.[65]

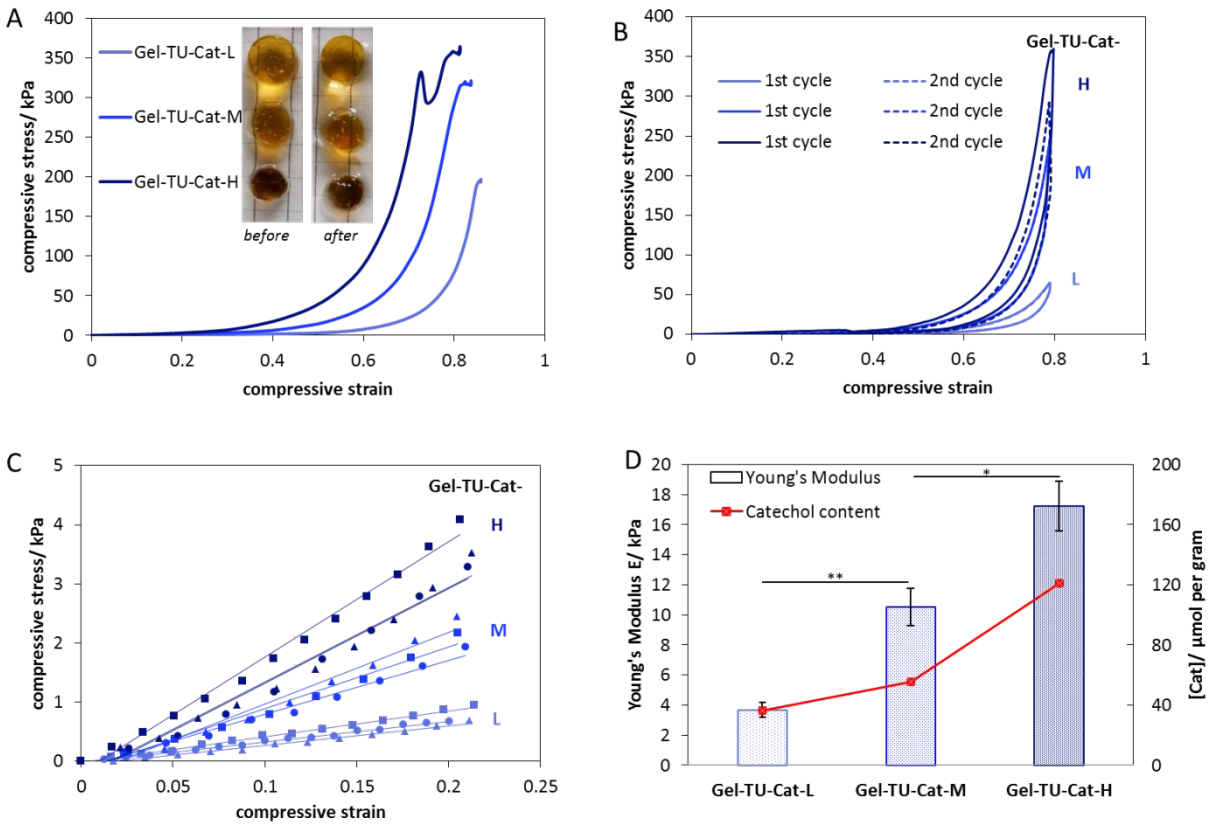

Figure 5. (A) Representative compressive stress-strain curves of Gel-TU-Cat hydrogels with inserted digital images of hydrogel disks before and after compressive tests. (B) Cyclic compressive tests with two consecutive loading-unloading cycles. (C) Linear fitting of the initial parts of the compressive tests with strain below 0.25 (n = 3, presented with square, circle or triangle symbols for each repeat). (D) Young's modulus of the hydrogels calculated from the linear fittings shown in panel C (*p<0.05, **p<0.01) and catechol contents ([Cat] µmol per gram polymer) of the Gel-TU-Cat polymers.

3.3 *Ex vivo* pericardium adhesion performance of Gel-TU-Cat hydrogels

The *in situ* formed Gel-TU-Cat hydrogels closely mimic soft tissues, both in terms of the Young's modulus and stress relaxation behaviors. To function as injectable hydrogel adhesive for tissue repair, they should also adhere strongly to the targeted tissue.[65] As a proof of concept, the *ex vivo* adhesion of the Gel-TU-Cat hydrogels on porcine pericardium tissues was investigated. Gel-TU-Cat-M hydrogels were selected due to their higher stability compared to Gel-TU-Cat-L hydrogels (Figure S12) and better ductility compared to Gel-TU-Cat-H

hydrogels (Figure 5). Two types of commercial adhesives were used for comparison, namely cyanoacrylate (CA) and TISSEEL (from Baxter) fibrin glues. The former is considered as the strongest available tissue adhesive, but only for closing small wounds on tissue surfaces due to its well-known cytotoxicity and exothermic gelation process.[19] The latter has been commonly used as hemostatic material during surgery.[66]

Adhesion strength of these *in situ* formed adhesives on pericardium surface was quantified with T-peeling tests, which is a standard test method for determining the adhesion strength of tissue adhesives (Figure 6A and Figure S4). Tension was applied horizontally to minimize the influence of gravity.[67] As expected, CA shows the highest adhesion energy (Figure 6B-C). However, the huge fluctuation of the peeling curve indicates the existence of significant interfacial inhomogeneity between solidified CA adhesive and the tissues surfaces (Figure 6B and Figure S13). This may have originated from the plastic-like nature of the rigid products from CA polymerization.[65, 68] In contrast, hydrogel adhesives with mechanical properties better resembling soft tissues provide more homogeneous adhesion on the tissue surface, as evidenced by much smoother peeling curves of Gel-TU-Cat-M and TISSEEL (Figure 6B). In addition, the adhesion energy of Gel-TU-Cat-M hydrogel adhesives (27.09 ± 2.50 J m^{-2}) was comparable to that of the commercial TISSEEL fibrin glue (24.92 ± 6.49 J m^{-2}, Figure 6C and Table S5).

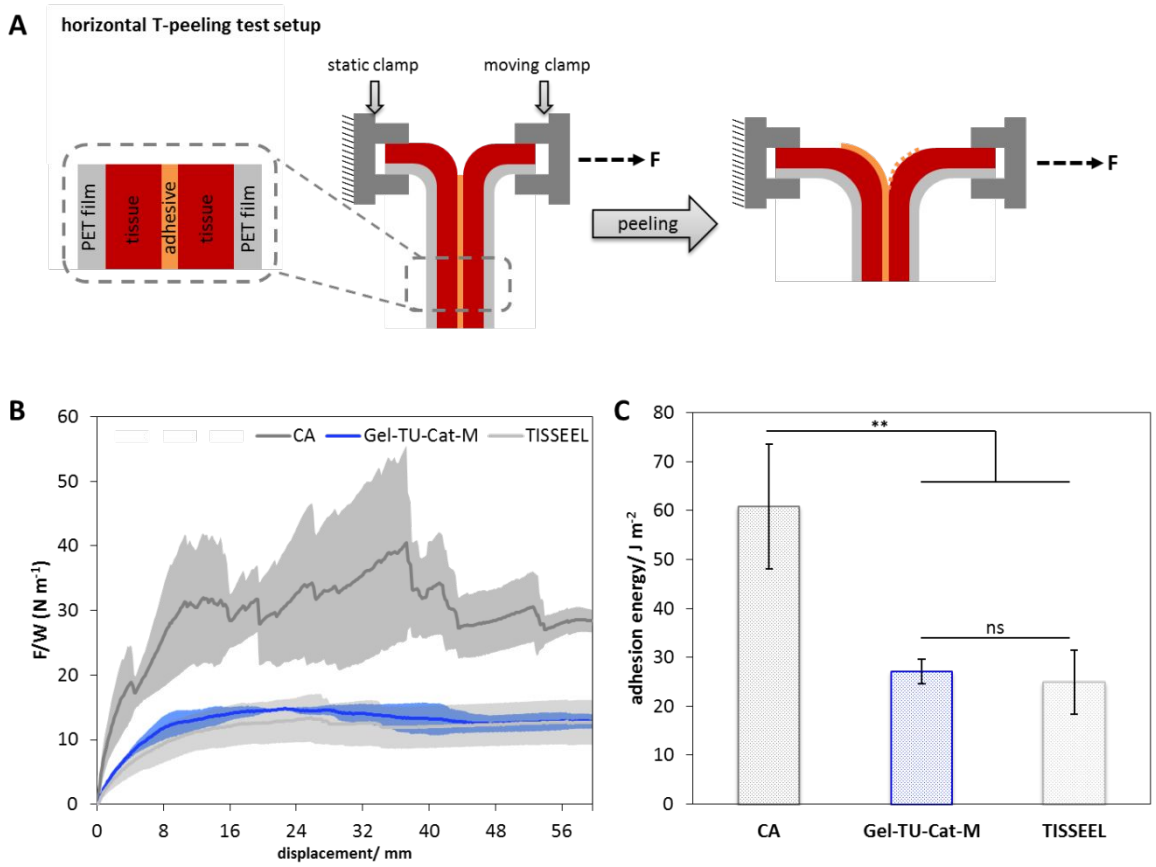

Figure 6. (A) Schematic illustration of the specimen for horizontal T-peeling tests. (B) Representative peeling curves (with confidence bands) of CA, Gel-TU-Cat-M and TISSEEL on pericardium tissue surfaces (F/W is the ratio of the force and width). (C) Adhesion energy of CA, Gel-TU-Cat-M and TISSEEL on pericardium tissue surfaces (**$p < 0.01$, ns: non-significant difference).

In order to further evaluate the tissue adhesion performance of the hydrogel adhesives on pericardium tissues, a more relevant standard test method for heart-related applications, i.e. bursting test, was used to compare the tissue adhesion performance of these three materials (Figure 7A and Figure S5). It is noteworthy that, different from the thin adhesive layers sealed between two tissue specimens in the T-peeling test setup, the adhesive-tissue interface in a burst test setup is continuously exposed to the pressuring fluid, which better resembles the conditions of heart-related applications. In agreement with the T-peeling test results, CA showed the strongest burst resistance with bursting pressure as high as 232.34 ± 46.11mmHg (Figure 7B-

C). However, although the adhesion energy of Gel-TU-Cat-M was found to be not significantly higher than that of the TISSEEL (Figure 6C), their bursting resistance was significantly stronger (Figure 7B-C). The bursting pressure of Gel-TU-Cat-M (127.31 ± 49.82 mmHg) was more than double that of the TISSEEL (53.69 ± 21.28 mmHg, Table S6). This could be ascribed to the covalent and non-covalent interactions between Gel-TU-Cat hydrogels and tissues as illustrated in Figure 1B, which are commonly found in catechol-containing adhesives.[36, 37] On the contrary, the formation of fibrin glues was reported to have a blood-clotting mechanism lacking significant covalent interactions with tissues in the absence of blood.[69, 70] It is noteworthy that, although Gel-TU-Cat-M hydrogels can withstand the normal human arterial blood pressure range (80–120 mmHg),[19] they are not strong enough to be used alone for sealing heart tissue defects. To be used for suture-free cardiovascular tissue sealing, tissue adhesives should withstand at least hypertensive peak pressure values that can reach 300 mmHg in some extreme cases.[24] Furthermore, the adhesion between hydrogels and tissues may be affected significantly by unexpected leaking of body fluids at physiological temperature. To mimic such a situation where the tissue adhesives are exposed to excessive body fluids under physiological temperature, we immersed the whole burst test setup in a 37 °C PBS bath. After being immersed in PBS for 15 minutes, a decrease of adhesion strength was found for CA and Gel-TU-Cat-M on pericardium tissues, indicating the loss of adhesive-tissue interfacial interactions. However, an unexpected increase of the bursting pressure between TISSEEL and pericardium tissues was found (Figure S14). Such a phenomenon indicates the possible complication of tissue adhesive applications, however, has rarely been investigated in the literature. We believe that exposure to body fluids should be taken into consideration when evaluating tissue adhesives for internal applications rather than for skin applications. Based on these results, Gel-TU-Cat injectable hydrogels show great promise to be used for delivery and anchorage of therapeutic agents to diseased tissues without fully penetrating defects. In the case of fully penetrating defects such

as incisions and punctures, they could be used complementary to conventional wound closure methods such as sutures and staples.

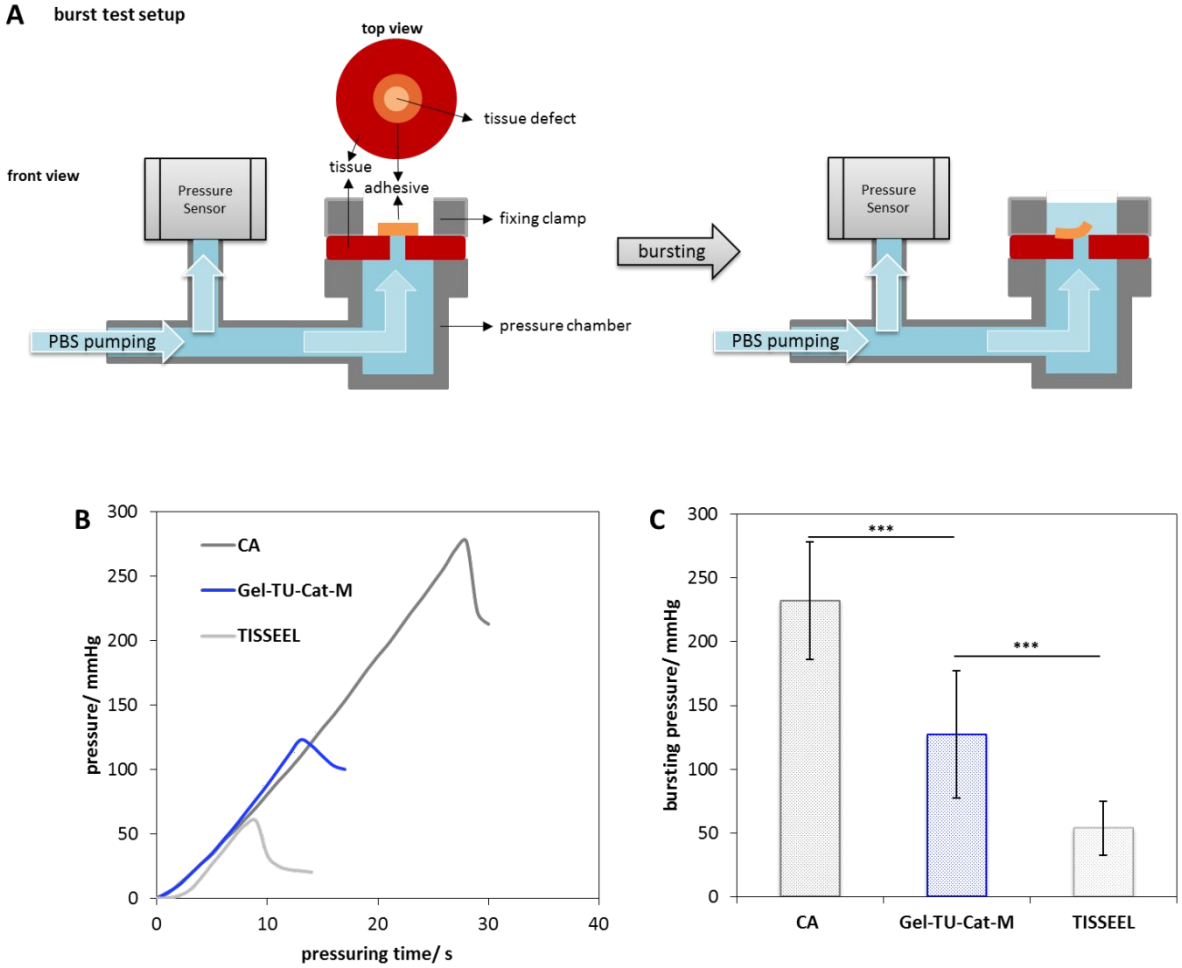

Figure 7. (A) Schematic illustration of the bursting test setup. (B) Representative bursting curves of CA, Gel-TU-Cat-M and TISSEEL on pericardium tissue surfaces. (C) Average bursting strength of CA, Gel-TU-Cat-M and TISSEEL on pericardium tissues (***$p < 0.001$).

3.4 Cytocompatibility and cell-remodeling of the Gel-TU-Cat-M hydrogels

The fast gelation behavior, soft tissue-mimicking matrix and hydrogel-tissue adhesion strength of Gel-TU-Cat hydrogels make them a very promising candidate for tissue repair applications. To further explore the use of such injectable hydrogel adhesives as cell-delivery biomaterials for tissue repair, we evaluated the cytocompatibility of the hydrogel material and the double-syringe injection delivery method. Normal human dermal fibroblasts (NHDFs) were encapsulated in 3D Gel-TU-Cat-M hydrogels via double-syringe injection (Figure S6) and

cultivated for up to 7 days. Cell-free and cell-laden hydrogels showed similar swelling behaviors, indicating that the encapsulation of cells has a negligible influence on hydrogel stability and mechanical properties (Figure S15). The high cytocompatibility of the hydrogel materials and double-syringe injection method was confirmed by live/dead staining after 24 hours of culture (Figure 8A and Figure S7). As presented in Figure 8C, hydrogels showed very low cytotoxicity with LDH release values of 3.81%, 4.65% and 2.67% at day 1, 3 and day 7, respectively. Notably, only a slightly higher LDH release from the hydrogel than that from the tissue culture plate (TCP) controls was observed on day 1, no significant difference was detected at days 3 and 7, thus confirming the excellent cytocompatibility of the hydrogel materials and the double-syringe injection method. Extensive spreading of NHDFs after 7 days of culture was observed, which indicates that the biochemical properties of native gelatin are preserved to support cell attachment and local degradation of the matrix (Figure 8B).[71, 72] . In addition, 2D cell culturing experiments showed extensive attachment and spreading of human umbilical vein endothelial cells (HUVECs) on Gel-TU-Cat-M hydrogels (Figure S16). Taken together, these results indicate that Gel-TU-Cat hydrogels can deliver living cells to target tissues via a minimally invasive double-syringe injection method, making them a promising biomaterial for cell-based repair of tissues, including cardiovascular tissues. It is noteworthy that, although the hydrogels remained intact during *in vitro* cell cultivation, their degradation strongly depends on the eventual site of *in vivo* application and the microenvironment. Therefore, *in vivo* investigation of hydrogel stability and degradation is the logical next step in future.

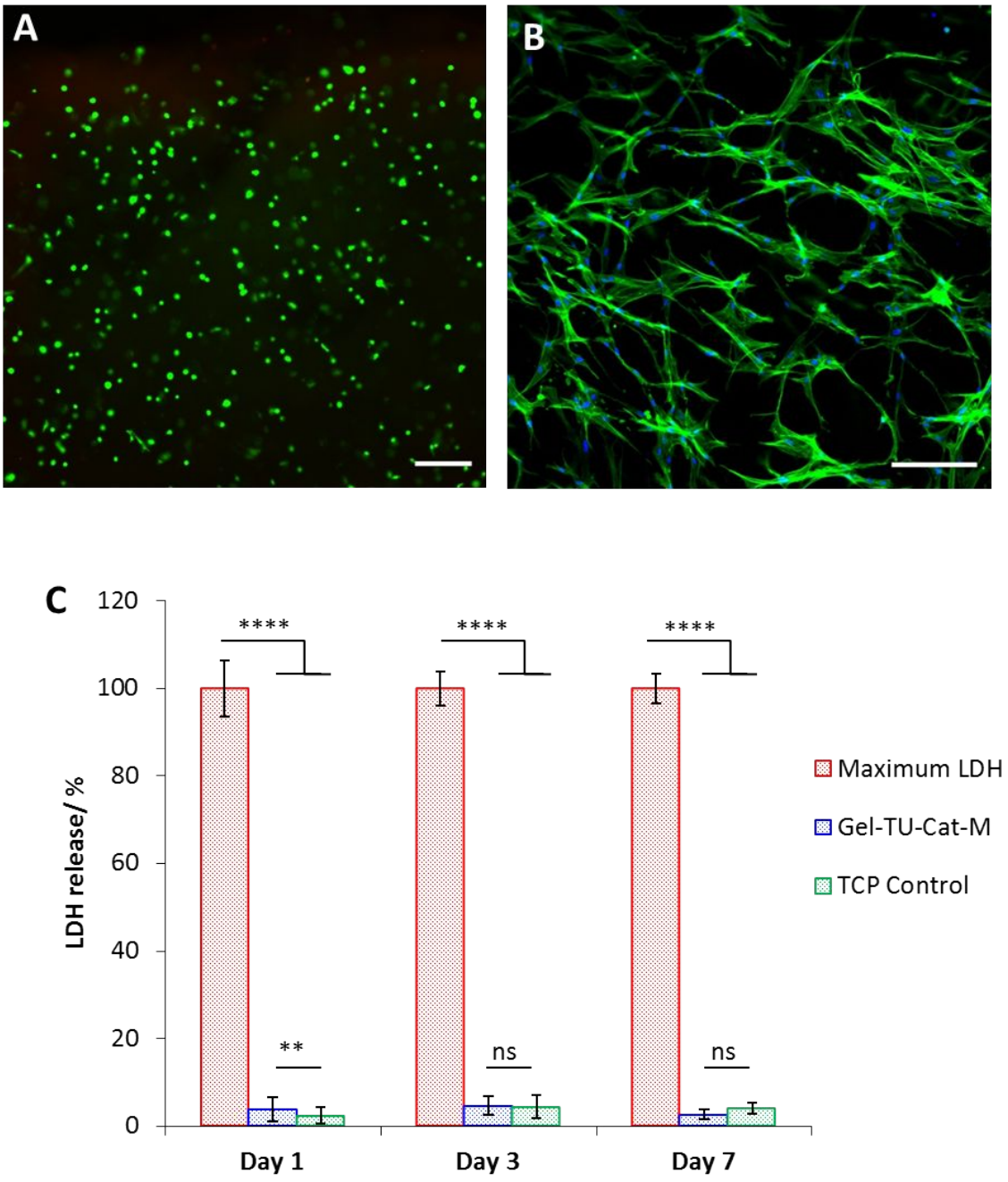

Figure 8. (A) Live/dead staining of normal human dermal fibroblasts (NHDFs) cultivated in 3D Gel-TU-Cat-M hydrogel matrix for 24 h (live: green; dead: red). (B) Confocal image of NHDFs cultivated in 3D Gel-TU-Cat-M hydrogel matrix for 7 days after staining of F-actin filaments (green) and cell nuclei (blue). (C) Cytotoxicity was assessed by measuring LDH release at day 1, 3 and day 7. **p < 0.01, ****p < 0.0001, ns for non-significant difference. Scale bars in panel A and B: 200 µm.

4. Conclusion

In this study, we report a mild and highly efficient crosslinking strategy for mussel-inspired tissue adhesives, which gives access to stable and cytocompatible hydrogels with near-native tissue properties. Unlike other mussel-inspired polymers with high catechol contents (e.g. PEG-DOPAs: ~286.7 μmol/g polymer, Supporting information: Supplementary Note 3) and non-reactive linkages that form hydrogels within minutes,[29] Gel-TU-Cat polymers with much lower catechol contents (~36 μmol/g) can be crosslinked rapidly (within 10 seconds) under mild conditions (Movie S1), thanks to the Mfp-6-mimicking nucleophilic thiourea (TU) linkages.[38, 39] This unique feature avoids the usage of toxic oxidants such as sodium periodate and therefore allows the injectable hydrogels to deliver living cells. Moreover, the preservation of catechol structures provides non-covalent crosslinking to the mussel-inspired hydrogel, making it a close mimic of soft tissues in terms of good ductility, similar elastic modulus and dual-mode stress relaxation behaviors. To the best of our knowledge, this discovery has never been reported in other mussel-inspired hydrogel systems. While minor modification of the cost-effective gelatin biopolymer imparts a collective of versatile properties to the tissue adhesive hydrogels, it barely interferes with the cell-binding motifs allowing extensive spreading of the encapsulated cells. These properties of Gel-TU-Cat hydrogel make it amenable to a diversity of applications in regenerative medicine and warranting further *in vivo* evaluation as a logical next step towards future clinical application.

ASSOCIATED CONTENT

Supporting Information.

The following files are available free of charge.

Synthesis and ^{1}H NMR characterization of DOPA-ITC (Figure S1); UV-vis spectra (Figure S2); Influence of H_2O_2 concentration on gelation rate (Figure S3); Schematic illustration of

the T-peeling tests (Figure S4); Schematic illustration of the bursting strength measurement (Figure S5); Schematic illustration and a digital image of the experimental setup for preparation of cell-laden hydrogel disk (Figure S6); Dead cell control of live/dead staining (Figure S7); Rheological frequency sweep and time sweep measurements (Figure S8); Influence of polymer or H2O2 concentration on hydrogel mechanical properties (Figure S9); SEM image of Gel-TU-Cat-H hydrogel (Figure S10); Consecutive loading-unloading compressive measurements (Figure S11); Swelling test of Gel-TU-Cat hydrogels (Figure S12); Representative peeling curves (Figrue S13); Representative bursting curves (Figure S14); Swelling behaviors of cell-free Gel-TU-Cat-M hydrogels in PBS and cell-laden Gel-TU-Cat-M hydrogels in culture medium (Figure S15); Confocal images of HUVECs (Figure S16); Fitting the stress relaxation data to the Maxwell-Weichert model (Supplementary Note 1); Calculation of Young's modulus (Supplementary Note 2); Catechol content of PEG-DOPAs from reference #29 (Supplementary Note 3); Normalized absorbance of DOPA-ITC standard solutions (Table S1); Normalized absorbance of Gel-TU-Cat solutions (Table S2); Best-fit parameters of stress relaxation obtained with double exponential decay (Table S3); Fitting parameters of the initial part of the compressive stress-strain curves (Table S4); Statistical analysis of T-Peeling data (Table S5); Statistical analysis of bursting pressure data (Table S6) (PDF)

The tube inversion test revealing the fast gelation of Gel-TU-Cat-L (movie S1) (avi)

AUTHOR INFORMATION

Corresponding Authors

*Email: claudio.toncelli@empa.ch (Dr. Claudio Toncelli); markus.rottmar@empa.ch (Dr. Markus Rottmar)

ORCID

Kongchang Wei: 0000-0002-6555-2768

Berna Senturk: 0000-0002-0116-7596

Martin T. Matter: 0000-0003-0748-1508

Inge K. Herrmann: 0000-0002-3018-6796

Markus Rottmar: 0000-0001-7636-428X

Claudio Toncelli: 0000-0003-3903-4972

Author Contributions

The manuscript was written through contributions of all authors. All authors have given approval to the final version of the manuscript. # These authors contributed equally.

Funding Sources

The project is supported by the EMPAPOSTDOCS-II program. The EMPAPOSTDOCS-II program has received funding from the European Union's Horizon 2020 research and innovation program under the Marie Skłodowska-Curie grant agreement number 754364.

ACKNOWLEDGMENT

We thank Mr. Roman Hinder and his colleagues from Slaughterhouse St. Gallen AG (operation Bazenheid) for kindly supplying fresh porcine hearts. We also thank Dr. Giuseppino Fortunato, Dr. Luciano F. Boesel, Dr. Katharina Maniura-Weber and Dr. René M. Rossi for helpful discussions on the current topic.

REFERENCES

(1) Seliktar, D. Designing Cell-Compatible Hydrogels for Biomedical Applications. *Science* **2012,** *336*, 1124-1128.

(2) Lee, K. Y.; Mooney, D. J. Hydrogels for Tissue Engineering. *Chem. Rev.* **2001,** *101*, 1869-1879.

(3) Zhang, Y. S.; Khademhosseini, A. Advances in Engineering Hydrogels. *Science* **2017,** *356*, eaaf3627.

(4) Wichterle, O.; Lím, D. Hydrophilic Gels for Biological Use. *Nature* **1960,** *185*, 117-118.

(5) Yu, L.; Ding, J. D. Injectable Hydrogels as Unique Biomedical Materials. *Chem. Soc. Rev.* **2008,** *37*, 1473-1481.

(6) Li, Y. L.; Rodrigues, J.; Tomas, H. Injectable and Biodegradable Hydrogels: Gelation, Biodegradation and Biomedical Applications. *Chem. Soc. Rev.* **2012,** *41*, 2193-2221.

(7) Mathew, A. P.; Uthaman, S.; Cho, K. H.; Cho, C. S.; Park, I. K. Injectable Hydrogels for Delivering Biotherapeutic Molecules. *Int. J. Biol. Macromol.* **2018,** *110*, 17-29.

(8) Liu, Y.; Meng, H.; Konst, S.; Sarmiento, R.; Rajachar, R.; Lee, B. P. Injectable Dopamine-Modified Poly(ethylene glycol) Nanocomposite Hydrogel with Enhanced Adhesive Property and Bioactivity. *ACS Appl. Mater. Interfaces* **2014,** *6*, 16982-16992.

(9) Lee, F.; Chung, J. E.; Kurisawa, M. An Injectable Hyaluronic Acid-Tyramine Hydrogel System for Protein Delivery. *J. Controlled Release* **2009,** *134*, 186-193.

(10) Cai, L.; Dewi, R. E.; Heilshorn, S. C. Injectable Hydrogels with In Situ Double Network Formation Enhance Retention of Transplanted Stem Cells. *Adv. Funct. Mater.* **2015,** *25*, 1344-1351.

(11) Lu, S. Y.; Gao, C. M.; Xu, X. B.; Bai, X.; Duan, H. G.; Gao, N. N.; Feng, C.; Xiong, Y.; Liu, M. Z. Injectable and Self-Healing Carbohydrate-Based Hydrogel for Cell Encapsulation. *ACS Appl. Mater. Interfaces* **2015,** *7*, 13029-13037.

(12) Liang, K.; Bae, K. H.; Kurisawa, M., Recent Advances in The Design of Injectable Hydrogels for Stem Cell-Based Therapy. *J. Mater. Chem. B* **2019**, *7,* 3775-3791.

(13) Chen, Y. P.; Luan, J. B.; Shen, W. J.; Lei, K. W.; Yu, L.; Ding, J. D. Injectable and Thermosensitive Hydrogel Containing Liraglutide as a Long-Acting Antidiabetic System. *ACS Appl. Mater. Interfaces* **2016,** *8*, 30703-30713.

(14) Huynh, V.; Wylie, R. G. Displacement Affinity Release of Antibodies from Injectable Hydrogels. *ACS Appl. Mater. Interfaces* **2019,** *11*, 30648-30660.

(15) Nguyen, Q. V.; Huynh, D. P.; Park, J. H.; Lee, D. S. Injectable Polymeric Hydrogels for The Delivery of Therapeutic Agents: A Review. *Eur. Polym. J.* **2015,** *72*, 602-619.

(16) Chen, W.; Yung, B. C.; Qian, Z. Y.; Chen, X. Y. Improving Long-term Subcutaneous Drug Delivery by Regulating Material-Bioenvironment Interaction. *Adv. Drug Delivery Rev.* **2018,** *127*, 20-34.

(17) Feng, Q.; Wei, K. C.; Lin, S. E.; Xu, Z.; Sun, Y. X.; Shi, P.; Li, G.; Bian, L. M. Mechanically Resilient, Injectable, and Bioadhesive Supramolecular Gelatin Hydrogels Crosslinked by Weak Host-Guest Interactions Assist Cell Infiltration and In Situ Tissue Regeneration. *Biomaterials* **2016,** *101*, 217-228.

(18) Mazza, E.; Ehret, A. E. Mechanical Biocompatibility of Highly Deformable Biomedical Materials. *J. Mech. Behav. Biomed. Mater.* **2015,** *48*, 100-124.

(19) Li, J.; Celiz, A. D.; Yang, J.; Yang, Q.; Wamala, I.; Whyte, W.; Seo, B. R.; Vasilyev, N. V.; Vlassak, J. J.; Suo, Z.; Mooney, D. J. Tough Adhesives for Diverse Wet Surfaces. *Science* **2017,** *357*, 378-381.

(20) Mandell, S. P.; Gibran, N. S. Fibrin Sealants: Surgical Hemostat, Sealant and Adhesive. *Expert Opin. Biol. Ther.* **2014,** *14*, 821-830.

(21) Wallace, D. G.; Cruise, G. M.; Rhee, W. M.; Schroeder, J. A.; Prior, J. J.; Ju, J.; Maroney, M.; Duronio, J.; Ngo, M. H.; Estridge, T.; Coker, G. C. A Tissue Sealant Based on Reactive Multifunctional Polyethylene Glycol. *J. Biomed. Mater. Res.* **2001,** *58*, 545-555.

(22) Zhu, J. M. Bioactive Modification of Poly(ethylene glycol) Hydrogels for Tissue Engineering. *Biomaterials* **2010,** *31*, 4639-4656.

(23) Assmann, A.; Vegh, A.; Ghasemi-Rad, M.; Bagherifard, S.; Cheng, G.; Sani, E. S.; Ruiz-Esparza, G. U.; Noshadi, I.; Lassaletta, A. D.; Gangadharan, S.; Tamayol, A.;

Khademhosseini, A.; Annabi, N. A Highly Adhesive and Naturally Derived Sealant. *Biomaterials* **2017,** *140*, 115-127.

(24) Annabi, N.; Zhang, Y. N.; Assmann, A.; Sani, E. S.; Cheng, G.; Lassaletta, A. D.; Vegh, A.; Dehghani, B.; Ruiz-Esparza, G. U.; Wang, X. C.; Gangadharan, S.; Weiss, A. S.; Khademhosseini, A. Engineering a Highly Elastic Human Protein-Based Sealant for Surgical Applications. *Sci. Transl. Med.* **2017,** *9*, eaai7466.

(25) Hong, Y.; Zhou, F.; Hua, Y.; Zhang, X.; Ni, C.; Pan, D.; Zhang, Y.; Jiang, D.; Yang, L.; Lin, Q.; Zou, Y.; Yu, D.; Arnot, D. E.; Zou, X.; Zhu, L.; Zhang, S.; Ouyang, H. A Strongly Adhesive Hemostatic Hydrogel for The Repair of Arterial and Heart Bleeds. *Nat. Commun.* **2019,** *10*, 2060.

(26) Waite, J. H.; Tanzer, M. L. Polyphenolic Substance of Mytilus Edulis: Novel Adhesive Containing L-DOPA and Hydroxyproline. *Science* **1981**, *212*, 1038-1040.

(27) Lee, B. P.; Messersmith, P. B.; Israelachvili, J. N.; Waite, J. H. Mussel-Inspired Adhesives and Coatings. *Annu. Rev. Mater. Res.* **2011***, 41*, 99-132.

(28) Moulay, S. Dopa/Catechol-Tethered Polymers: Bioadhesives and Biomimetic Adhesive Materials. *Polym. Rev.* **2014,** *54*, 436-513.

(29) Lee, B. P.; Dalsin, J. L.; Messersmith, P. B. Synthesis and Gelation of DOPA-Modified Poly(ethylene glycol) Hydrogels. *Biomacromolecules* **2002,** *3*, 1038-1047.

(30) Brubaker, C. E.; Messersmith, P. B. Enzymatically Degradable Mussel-Inspired Adhesive Hydrogel. *Biomacromolecules* **2011,** *12*, 4326-4334.

(31) Ryu, J. H.; Lee, Y.; Kong, W. H.; Kim, T. G.; Park, T. G.; Lee, H. Catechol-Functionalized Chitosan/Pluronic Hydrogels for Tissue Adhesives and Hemostatic Materials. *Biomacromolecules* **2011,** *12*, 2653-2659.

(32) Brubaker, C. E.; Kissler, H.; Wang, L. J.; Kaufman, D. B.; Messersmith, P. B. Biological Performance of Mussel-Inspired Adhesive in Extrahepatic Islet Transplantation. *Biomaterials* **2010,** *31*, 420-427.

(33) Burke, S. A.; Ritter-Jones, M.; Lee, B. P.; Messersmith, P. B. Thermal Gelation and Tissue Adhesion of Biomimetic Hydrogels. *Biomed. Mater.* **2007,** *2*, 203-210.

(34) Yu, J.; Wei, W.; Danner, E.; Ashley, R. K.; Israelachvili, J. N.; Waite, J. H. Mussel Protein Adhesion Depends on Interprotein Thiol-Mediated Redox Modulation. *Nat. Chem. Biol.* **2011,** *7*, 588-590.

(35) Waite, J. H. Mussel Adhesion - Essential Footwork. *J. Exp. Biol.* **2017,** *220*, 517-530.

(36) Ahn, B. K. Perspectives on Mussel-Inspired Wet Adhesion. *J. Am. Chem. Soc.* **2017,** *139*, 10166-10171.

(37) Saiz-Poseu, J.; Mancebo-Aracil, J.; Nador, F.; Busque, F.; Ruiz-Molina, D. The Chemistry behind Catechol-Based Adhesion. *Angew. Chem., Int. Ed.* **2019,** *58*, 696-714.

(38) Horsch, J.; Wilke, P.; Pretzler, M.; Seuss, M.; Melnyk, I.; Remmler, D.; Fery, A.; Rompel, A.; Borner, H. G. Polymerizing Like Mussels Do: Toward Synthetic Mussel Foot Proteins and Resistant Glues. *Angew. Chem., Int. Ed.* **2018,** *57*, 15728-15732.

(39) Xu, Y. J.; Wei, K. C.; Zhao, P. C.; Feng, Q.; Choi, C. K. K.; Bian, L. M. Preserving The Adhesion of Catechol-Conjugated Hydrogels by Thiourea-Quinone Coupling. *Biomater. Sci.* **2016,** *4*, 1726-1730.

(40) Medintz, I. L.; Stewart, M. H.; Trammell, S. A.; Susumu, K.; Delehanty, J. B.; Mei, B. C.; Melinger, J. S.; Blanco-Canosa, J. B.; Dawson, P. E.; Mattoussi, H. Quantum-Dot/Dopamine Bioconjugates Function as Redox Coupled Assemblies for in vitro and Intracellular pH Sensing. *Nat. Mater.* **2010,** *9*, 676-684.

(41) Kale, R.; Bajaj, A. Ultraviolet Spectrophotometric Method for Determination of Gelatin Crosslinking in The Presence of Amino Groups. *J. Young Pharm.* **2010,** *2*, 90-94.

(42) Smith, S. M.; Wunder, M. B.; Norris, D. A.; Shellman, Y. G., A Simple Protocol for Using a LDH-Based Cytotoxicity Assay to Assess The Effects of Death and Growth Inhibition at The Same Time. *PloS One* **2011,** *6*, e26908.

(43) Kumar, P.; Nagarajan, A.; Uchil, P. D., Analysis of Cell Viability by The Lactate Dehydrogenase Assay. *Cold Spring Harbor Protocols* **2018,** *2018*, 465-468.

(44) Mehdizadeh, M.; Weng, H.; Gyawali, D.; Tang, L. P.; Yang, J. Injectable Citrate-Based Mussel-Inspired Tissue Bioadhesives with High Wet Strength for Sutureless Wound Closure. *Biomaterials* **2012,** *33*, 7972-7983.

(45) Sakai, S.; Hirose, K.; Taguchi, K.; Ogushi, Y.; Kawakami, K. An Injectable, In Situ Enzymatically Gellable, Gelatin Derivative for Drug Delivery and Tissue Engineering. *Biomaterials* **2009,** *30*, 3371-3377.

(46) Khanmohammadi, M.; Dastjerdi, M. B.; Ai, A.; Ahmadi, A.; Godarzi, A.; Rahimi, A.; Ai, J. Horseradish Peroxidase-Catalyzed Hydrogelation for Biomedical Applications. *Biomater. Sci.* **2018***, 6*, 1286-1298.

(47) Asai, D.; Xu, D. H.; Liu, W. G.; Quiroz, F. G.; Callahan, D. J.; Zalutsky, M. R.; Craig, S. L.; Chilkoti, A. Protein Polymer Hydrogels by In Situ, Rapid and Reversible Self-Gelation. *Biomaterials* **2012,** *33*, 5451-5458.

(48) Benton, J. A.; DeForest, C. A.; Vivekanandan, V.; Anseth, K. S. Photocrosslinking of Gelatin Macromers to Synthesize Porous Hydrogels That Promote Valvular Interstitial Cell Function. *Tissue Eng., Part A* **2009,** *15*, 3221-3230.

(49) Billiet, T.; Van Gasse, B.; Gevaert, E.; Cornelissen, M.; Martins, J. C.; Dubruel, P. Quantitative Contrasts in the Photopolymerization of Acrylamide and Methacrylamide-Functionalized Gelatin Hydrogel Building Blocks. *Macromol. Biosci.* **2013,** *13*, 1531-1545.

(50) da Silva, M. A.; Bode, F.; Grillo, I.; Dreiss, C. A. Exploring the Kinetics of Gelation and Final Architecture of Enzymatically Cross-Linked Chitosan/Gelatin Gels. *Biomacromolecules* **2015,** *16*, 1401-1409.

(51) Van den Bulcke, A. I.; Bogdanov, B.; De Rooze, N.; Schacht, E. H.; Cornelissen, M.; Berghmans, H. Structural and Rheological Properties of Methacrylamide Modified Gelatin Hydrogels. *Biomacromolecules* **2000,** *1*, 31-38.

(52) Rahali, K.; Ben Messaoud, G.; Kahn, C. J. F.; Sanchez-Gonzalez, L.; Kaci, M.; Cleymand, F.; Fleutot, S.; Linder, M.; Desobry, S.; Arab-Tehrany, E. Synthesis and Characterization of Nanofunctionalized Gelatin Methacrylate Hydrogels. *Int. J. Mol. Sci.* **2017,** *18*, 2675.

(53) Lin, P.; Ma, S. H.; Wang, X. L.; Zhou, F. Molecularly Engineered Dual-Crosslinked Hydrogel with Ultrahigh Mechanical Strength, Toughness, and Good Self-Recovery. *Adv. Mater.* **2015,** *27*, 2054-2059.

(54) Sun, J. Y.; Zhao, X. H.; Illeperuma, W. R. K.; Chaudhuri, O.; Oh, K. H.; Mooney, D. J.; Vlassak, J. J.; Suo, Z. G. Highly Stretchable and Tough Hydrogels. *Nature* **2012,** *489*, 133-136.

(55) Yang, B. G.; Wei, Z.; Chen, X. Y.; Wei, K. C.; Bian, L. M. Manipulating The Mechanical Properties of Biomimetic Hydrogels with Multivalent Host-Guest Interactions. *J. Mater. Chem. B* **2019,** *7*, 1726-1733.

(56) Li, H. Q.; Liu, F. Y.; Li, Z. Y.; Wang, S. F.; Jin, R. H.; Liu, C. Y.; Chen, Y. M., Fingerprintable Hydrogel from Dual Reversible Cross-Linking Networks with Different Relaxation Times. *ACS Appl. Mater. Interfaces* **2019,** *11*, 17925-17930.

(57) Findley, W. N.; Davis, F. A. Creep and Relaxation of Nonlinear Viscoelastic Materials, with An Introduction to Linear Viscoelasticity. *North-Holland, New York,* **1976**.

(58) Lv, S.; Dudek, D. M.; Cao, Y.; Balamurali, M. M.; Gosline, J.; Li, H. B. Designed Biomaterials to Mimic The Mechanical Properties of Muscles. *Nature* **2010,** *465*, 69-73.

(59) Liu, J.; Tan, C. S. Y.; Yu, Z. Y.; Lan, Y.; Abell, C.; Scherman, O. A. Biomimetic Supramolecular Polymer Networks Exhibiting both Toughness and Self-Recovery. *Adv. Mater.* **2017,** *29*, 1604951.

(60) Wei, K. C.; Zhu, M.; Sun, Y.; Xu, J.; Feng, Q.; Lin, S.; Wu, T.; Xu, J.; Tian, F.; Xia, J.; Li, G.; Bian, L. Robust Biopolymeric Supramolecular "Host-Guest Macromer" Hydrogels Reinforced by In Situ Formed Multivalent Nanoclusters for Cartilage Regeneration. *Macromolecules* **2016,** *49*, 866-875.

(61) Wei, K. C.; Chen, X. Y.; Li, R.; Feng, Q.; Bian, L. M. Multivalent Host-Guest Hydrogels as Fatigue-Resistant 3D Matrix for Excessive Mechanical Stimulation of Encapsulated Cells. *Chem. Mater.* **2017,** *29*, 8604-8610.

(62) Zhao, X. H. Multi-Scale Multi-Mechanism Design of Tough Hydrogels: Building Dissipation into Stretchy Networks. *Soft Matter* **2014,** *10*, 672-687.

(63) Fung, Y. C. Biomechanics: Mechanical Properties of Living Tissues. *Springer Science & Business Media, New York,* **2013**.

(64) Engler, A. J.; Sen, S.; Sweeney, H. L.; Discher, D. E. Matrix Elasticity Directs Stem Cell Lineage Specification. *Cell* **2006,** *126*, 677-689.

(65) Mehdizadeh, M.; Yang, J. Design Strategies and Applications of Tissue Bioadhesives. *Macromol. Biosci.* **2013,** *13*, 271-288.

(66) Silver, F. H.; Wang, M. C.; Pins, G. D. Preparation and Use of Fibrin Glue in Surgery. *Biomaterials* **1995,** *16*, 891-903.

(67) Padhye, N.; Parks, D. M.; Slocum, A. H.; Trout, B. L. Enhancing the Performance of The T-Peel Test for Thin and Flexible Adhered Laminates. *Rev. Sci. Instrum.* **2016,** *87*, 085111.

(68) Vinters, H. V.; Galil, K. A.; Lundie, M. J.; Kaufmann, J. C. E. The Histotoxicity of Cyanoacrylates – A Selective Review. *Neuroradiology* **1985,** *27*, 279-291.

(69) Sierra, D. H. Fibrin Sealant Adhesive Systems: A Review of Their Chemistry, Material Properties and Clinical Applications. *J. Biomater. Appl.* **1993,** *7*, 309-352.

(70) Bouten, P. J. M.; Zonjee, M.; Bender, J.; Yauw, S. T. K.; van Goor, H.; van Hest, J. C. M.; Hoogenboom, R. The Chemistry of Tissue Adhesive Materials. *Prog. Polym. Sci.* **2014,** *39*, 1375-1405.

(71) Koshy, S. T.; Ferrante, T. C.; Lewin, S. A.; Mooney, D. J. Injectable, Porous, and Cell-Responsive Gelatin Cryogels. *Biomaterials* **2014,** *35*, 2477-2487.

(72) Yue, K.; Trujillo-de Santiago, G.; Alvarez, M. M.; Tamayol, A.; Annabi, N.; Khademhosseini, A. Synthesis, Properties, and Biomedical Applications of Gelatin Methacryloyl (GelMA) Hydrogels. *Biomaterials* **2015,** *73*, 254-271.

Graphic Abstract

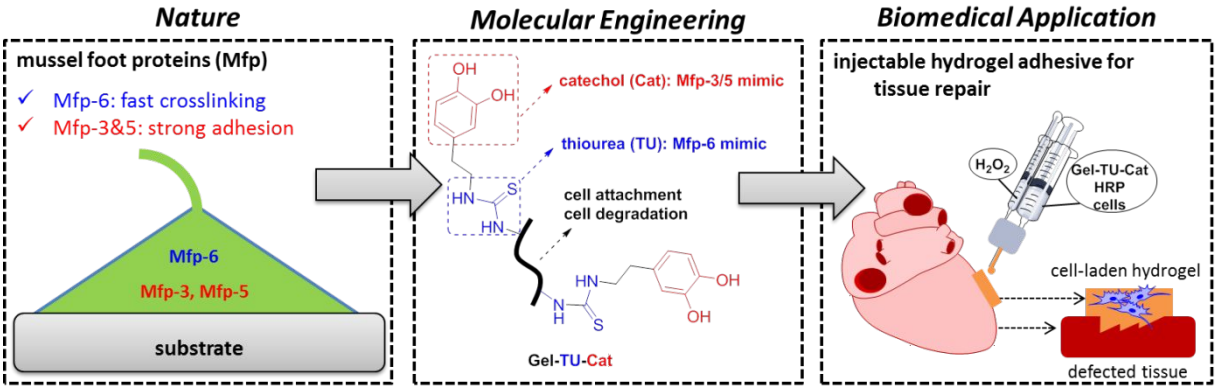

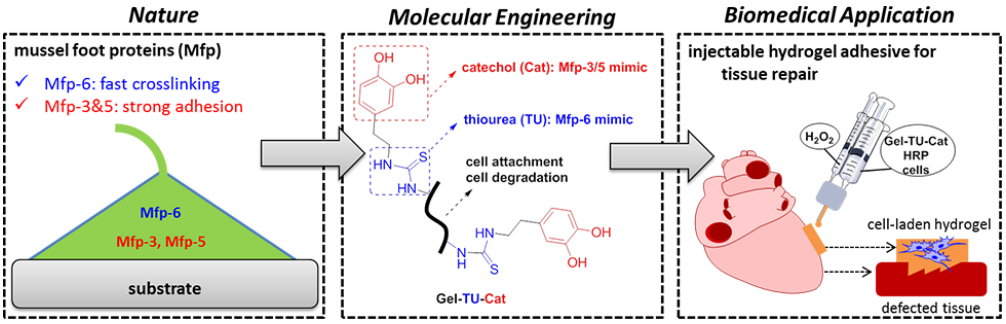

For Table of Content Only

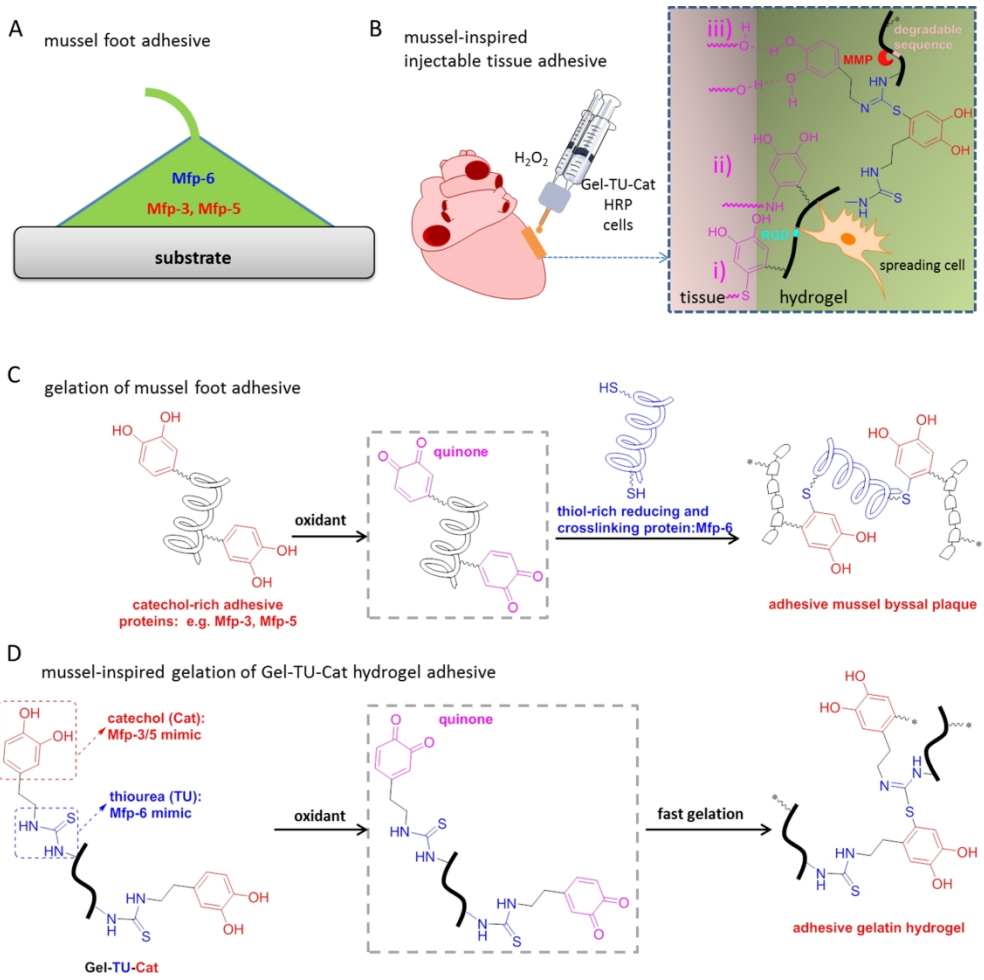

Figure 1. Schematic illustration of the mussel-inspired injectable Gel-TU-Cat hydrogel tissue adhesive. (A) Schematic of mussel foot proteins (Mfps) involved in strong mussel-substrate adhesion. (B) Relevant interfacial interactions (highlighted by pink structures: i. thiol-catechol addition, ii. amine-catechol addition and iii. hydrogen bonding) and cell spreading due to the presence of RGD and MMP-degradable sequence. (C) The formation of the adhesive mussel byssal plaques from catechol-rich adhesive proteins (e.g. Mfp-3 and Mfp-5) and thiol-rich re-ducing and crosslinking protein Mfp-6. (D) The biomimetic formation of crosslinked and ad-hesive Gel-TU-Cat hydrogel adhesive, of which the catechol (Cat) moieties mimic the adhe-sive function of Mfp-3 and Mfp-5, and the thiourea (TU) linkages mimic the reducing and crosslinking function of Mfp-6.

177x171mm (300 x 300 DPI)

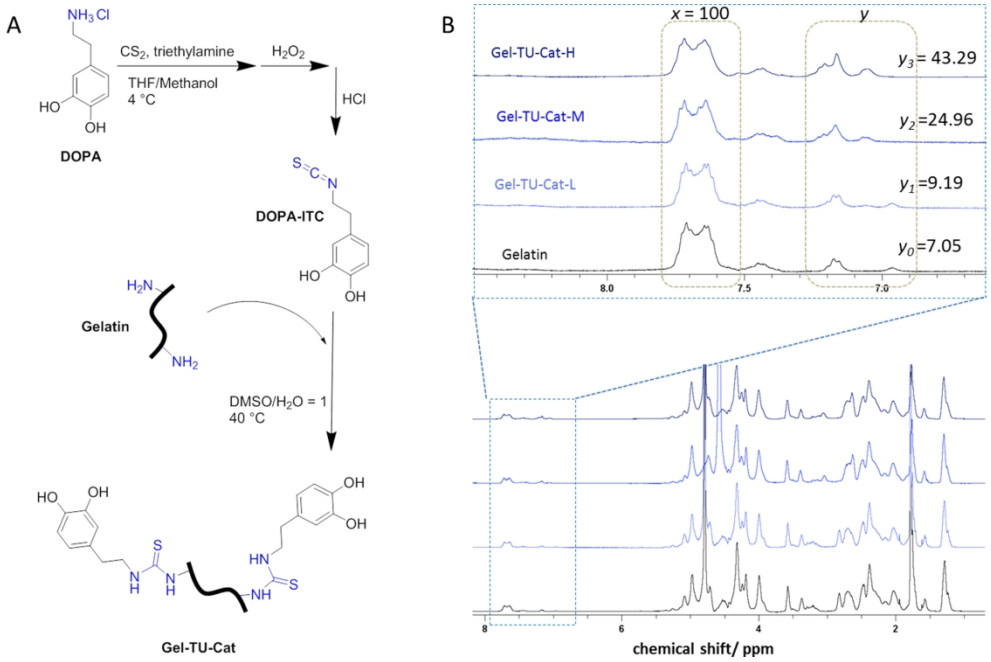

Figure 2. (A) Synthesis of Gel-TU-Cat polymers. (B) ^{1}H NMR characterization of gelatin and Gel-TU-Cat polymers (in D_2O, 37°C) with different functionalization degrees.

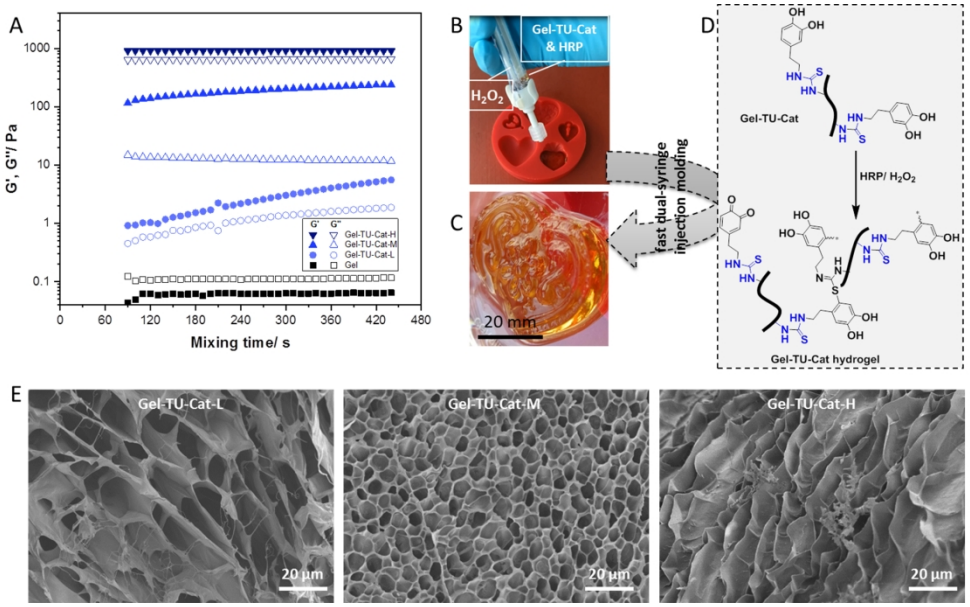

Figure 3. (A) Gelation of Gel-TU-Cat polymers characterized by rheological time sweep measurement. (B-D) Fast double-syringe injection molding of Gel-TU-Cat-M into a heart shaped object with sophisticated surface features from the mold. (E) SEM images showing the effect of functionalization degree on micro-structures of Gel-TU-Cat hydrogels.

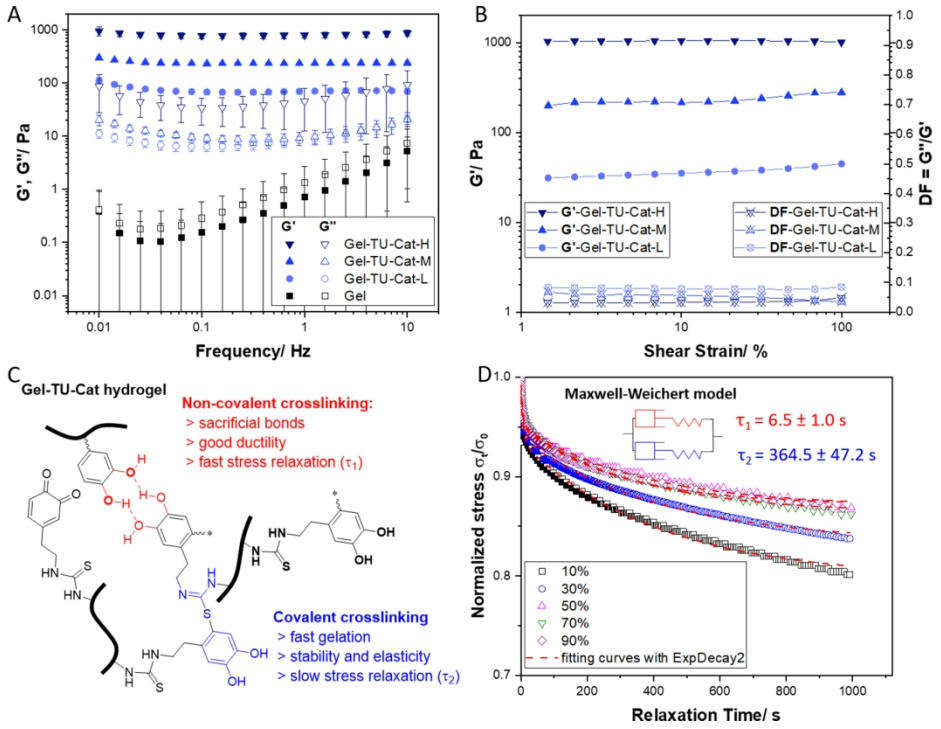

Figure 4. (A) Dynamic oscillatory rheological frequency-sweep measurements of Gel-TU-Cat or gelatin under enzymatic oxidation (n=3). (B) Dynamic oscillatory rheological amplitude-sweep measurements of Gel-TU-Cat hydrogels. (C) Schematic illustration of covalent and non-covalent hybrid crosslinking of the Gel-TU-Cat hydrogels. (D) Shear stress relaxation of Gel-TU-Cat-M hydrogels under different strains (10-90%) described by the Maxwell-Weichert model with two spring-dashpot Maxwell elements in parallel. The stress relaxation curves were fitted with double exponential decay, giving two characteristic relaxation times (τ1 and τ2) of the hydrogel. The rheological and stress relaxation measurements were carried out at 37 °C.

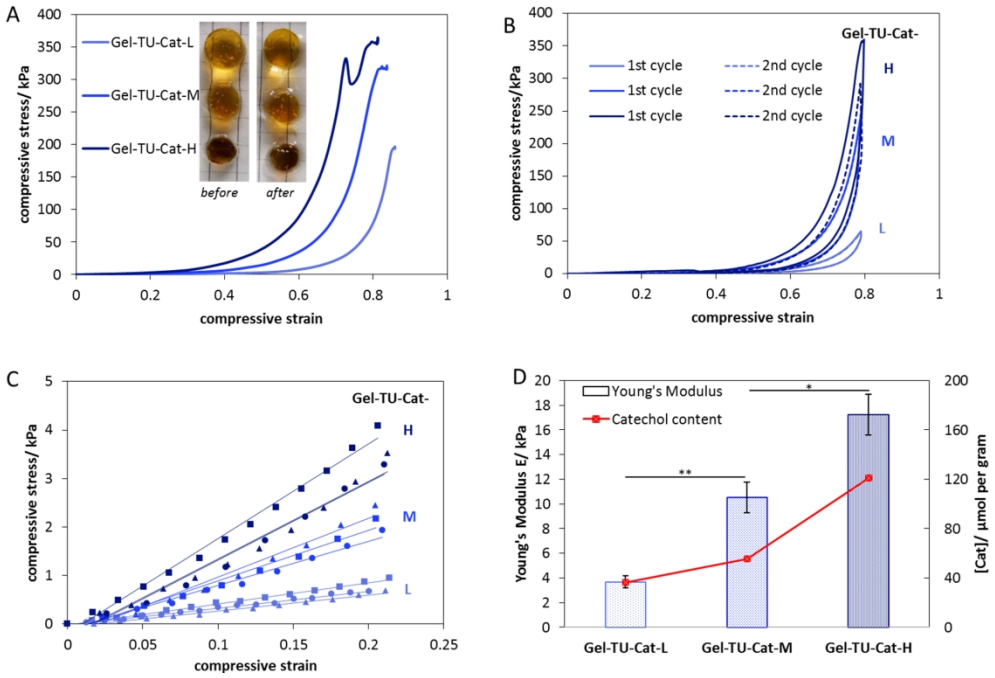

Figure 5. (A) Representative compressive stress-strain curves of Gel-TU-Cat hydrogels with inserted digital images of hydrogel disks before and after compressive tests. (B) Cyclic compressive tests with two consecutive loading-unloading cycles. (C) Linear fitting of the initial parts of the compressive tests with strain below 0.25 (n = 3, presented with square, circle or triangle symbols for each repeat). (D) Young's modulus of the hydrogels calculated from the linear fittings shown in panel C (*p<0.05, **p<0.01) and catechol contents ([Cat] µmol per gram polymer) of the Gel-TU-Cat polymers.

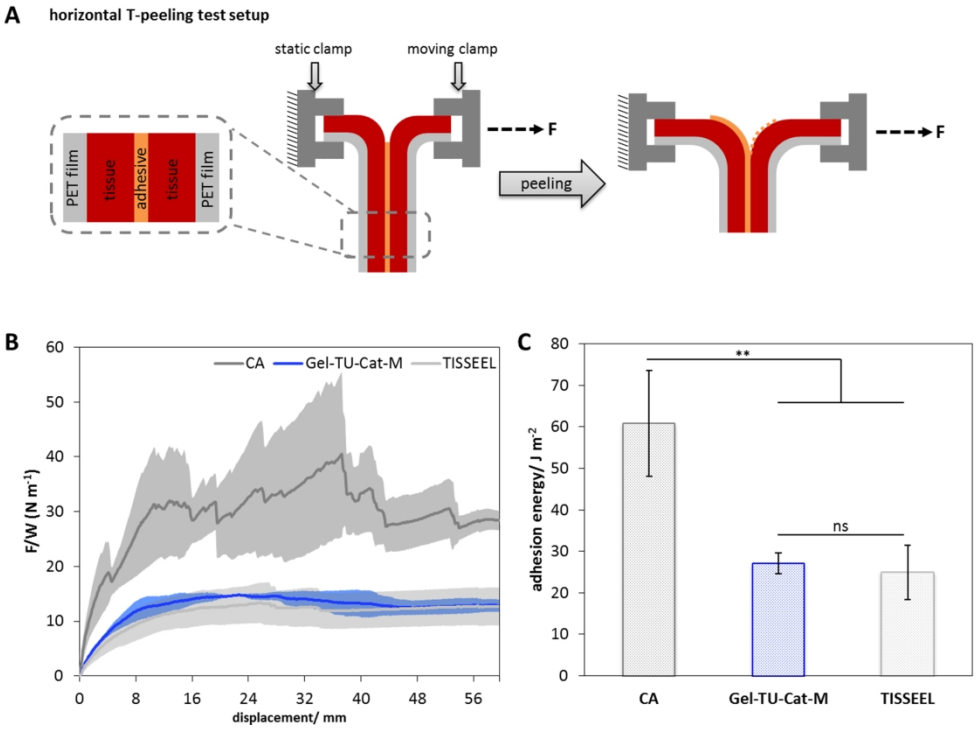

Figure 6. (A) Schematic illustration of the specimen for horizontal T-peeling tests. (B) Representative peeling curves (with confidence bands) of CA, Gel-TU-Cat-M and TISSEEL on per-icardium tissue surfaces (F/W is the ratio of the force and width). (C) Adhesion energy of CA, Gel-TU-Cat-M and TISSEEL on pericardium tissue surfaces (**p < 0.01, ns: non-significant difference).

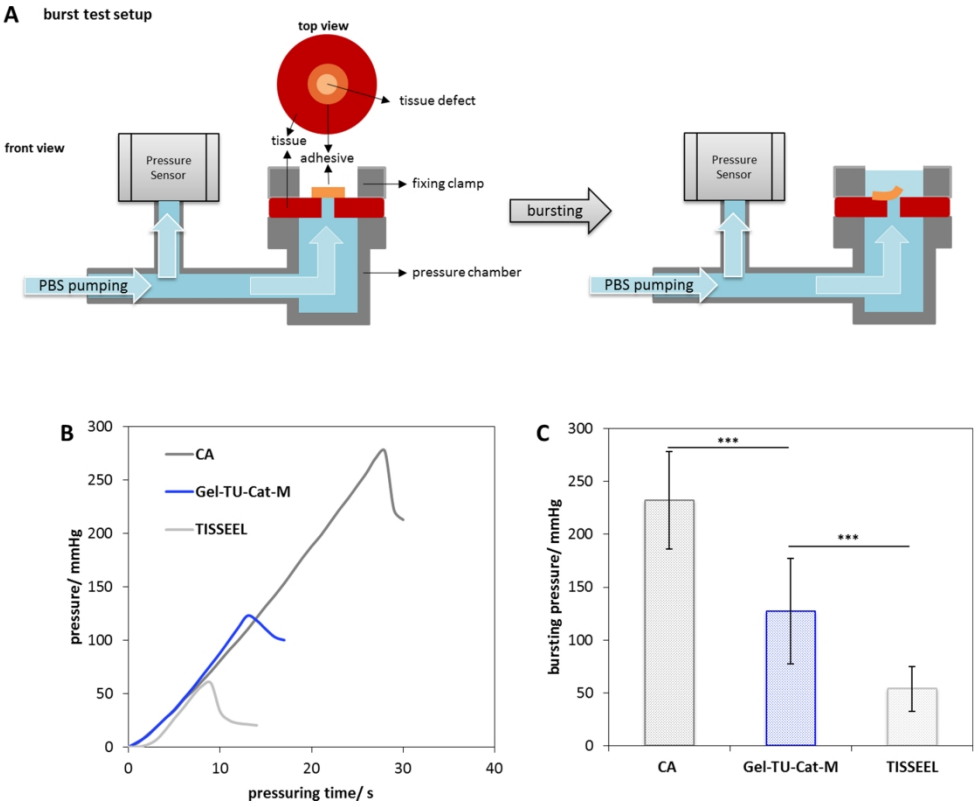

Figure 7. (A) Schematic illustration of the bursting test setup. (B) Representative bursting curves of CA, Gel-TU-Cat-M and TISSEEL on pericardium tissue surfaces. (C) Average bursting strength of CA, Gel-TU-Cat-M and TISSEEL on pericardium tissues (***$p < 0.001$).

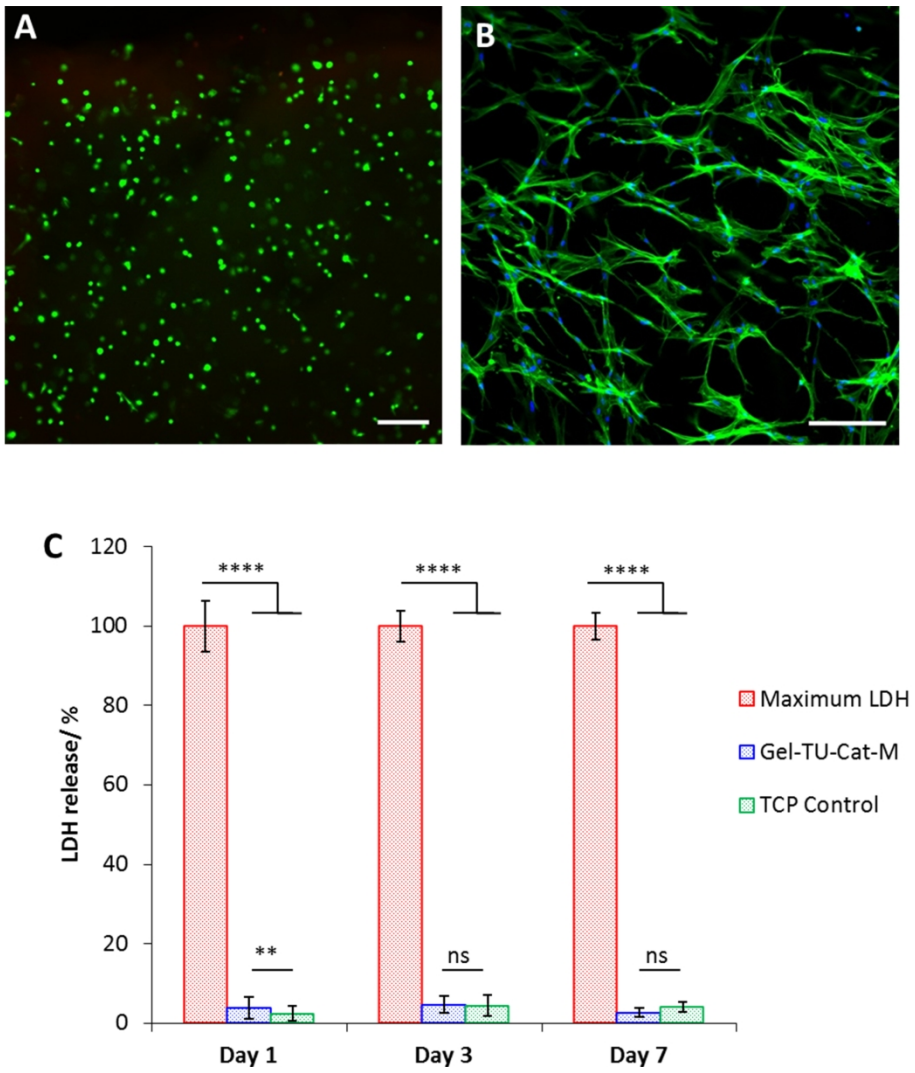

Figure 8. (A) Live/dead staining of normal human dermal fibroblasts (NHDFs) cultivated in 3D Gel-TU-Cat-M hydrogel matrix for 24 h (live: green; dead: red). (B) Confocal image of NHDFs cultivated in 3D Gel-TU-Cat-M hydrogel matrix for 7 days after staining of F-actin filaments (green) and cell nuclei (blue). (C) Cytotoxicity was assessed by measuring LDH release at day 1, 3 and day 7. **p < 0.01, ****p < 0.0001, ns for non-significant difference. Scale bars in panel A and B: 200 µm.